Polarization of the galactic 75-cm radiation

Westerhout, G.; Seeger, C.L.; Brouw, W.N.; Tinbergen, J.

BULLETIN OF THE ASTRONOMICAL INSTITUTES OF THE NETHERLANDS

1962 JULY 6 VOLUME XVI NUMBER 518

COMMUNICATIONS FROM THE OBSERVATORY AT LEIDEN AND THE NETHERLANDS FOUNDATION FOR RADIO ASTRONOMY

POLARIZATION OF THE GALACTIC 75-CM RADIATION

BY GART WESTERHOUT, CH. L. SEEGER, W. N. BROUW AND J. TINBERGEN

A description is given of a successful preliminary attempt to measure linear polarization in the continuous background radiation from the Galaxy. If the nonthermal radio emission is due to the synchrotron mechanism, such polarization is expected. The observed degree of polarization depends on the variation of the direction of the magnetic field and on the Faraday rotation along the line of sight. The observations were made with a linear polarimeter, using the 25-metre radio telescope at Dwingeloo. The feed consisted of a cylindrical waveguide section with two orthogonal probes. These were connected to two receivers, the output of which was phase-switched at the intermediate-frequency (50 Mc/s) stage. Each night a large number of control measurements were made of the polarization at the North pole, from which it was possible to deduce the instrumental polarization (Figure 5). It is shown that ionospheric Faraday rotation, although high just after sunset, rotates the direction of polarization by about 20° on the average. An attempt was made to remove the effects of spurious polarization from the measurements. The synchrotron emission of the VAN ALLEN belts and the interplanetary medium is shown to be negligible. The results are given in Figure 10. Polarized radiation of up to 6 °K and a degree of polarization of up to 10% are found. It is shown that interstellar Faraday rotation will depolarize radiation from behind an ionized interstellar cloud and therefore the observed radiation probably originates close to the sun. In some places there seems to be detailed agreement with optical observations. The observations were meant as a preliminary exploration. They cover only a very limited fraction of the sky, not even enough to decide whether some of the features seen in the continuous background radiation have a degree of polarization which is in any way remarkable. Our observations are compatible with earlier observations, some of which gave negative results.

1. *Introduction*

An electron moving in a homogeneous magnetic field will, unless its velocity is exactly parallel to the field, follow a helical path under the influence of the Lorentz force. At low electron velocities the radiation emitted in this process consists mainly of one frequency, the gyro-frequency $\nu_0 = eH/2\pi mc$. At velocities near the velocity of light, where the energy of the electron greatly exceeds the rest energy ($E \gg mc^2$), many harmonics of ν_0 are emitted, in practice forming a continuous spectrum with a maximum near the frequency $\nu_c = \nu_0 (E/mc^2)^2$.

This theory, some 50 years old, has received new attention within the last ten years because it provides an important mechanism for the emission of radiation at optical and radio wavelengths on a cosmic scale. This radiation is usually called synchrotron radiation, and sometimes radiation by magnetic deceleration, or magnetic bremsstrahlung. ALFVÉN and HERLOFSON (1950) and KIEPENHEUER (1950) first suggested this mechanism as the source of the nonthermal radio radiation in the sun and the Galaxy. In the following years the theory was developed in great detail by GINZBURG (1951, 1953) and collaborators, and applied extensively to radio-astronomical results by SHKLOVSKI (for a review of the theory, and an extensive list of references, see SHKLOVSKI 1960).

Verification of this theory turns out to be rather difficult. An important part of the continuous radio emission from our Galaxy is nonthermal. One indication that this part must be explained as being due to the synchrotron mechanism follows from the spectrum; the energy spectrum of the radiating electrons, derived from the spectrum of the radio emission, agrees fairly well with the energy spectrum of

CONTENTS

the positive cosmic ray particles. The most certain verification would be given by a direct measurement of the strength of the magnetic field in the Galaxy, and of the electron content of the primary cosmic rays. Until such experiments are possible, however, we shall have to find less direct evidence.

This may be found in the nonthermal radiation itself, which should be linearly polarized if it originates in the synchrotron emission from relativistic electrons (for theory see WESTFOLD 1959, LE ROUX 1961). The plane of vibration of the electric vector should, according to the theory, be perpendicular to the projection of the direction of the magnetic field on the sky. The degree of polarization is expected to be small, since it seems unlikely that the magnetic field has the same direction everywhere along the line of sight. Also, at the frequencies where nonthermal radiation contributes the major portion of the total radiation, i.e. at $\nu < 1000$ Mc/s, Faraday rotation due to the presence of ionized gas in the galactic magnetic field will affect the degree of polarization.

Measurement of the polarization of the radiation would be of great importance. Attempts to detect polarization have been made by RAZIN (1958), THOMSON (1957), PAWSEY and HARTING (1960) and PAULINY-TOTH, BALDWIN and SHAKESHAFT (1961). RAZIN and THOMSON obtain positive results. RAZIN finds a degree of polarization of 2 to 4 per cent at 207 Mc/s; THOMSON finds 1 per cent at 160 Mc/s; the other authors give upper limits of 1 to 2 per cent at frequencies between 200 and 410 Mc/s.

The measurements described in the present paper were made at a frequency of 408 Mc/s with the 25-metre radio telescope of the Netherlands Foundation for Radio Astronomy at Dwingeloo. The beamwidth was 2°, the bandwidth 1.9 Mc/s. The observations were made between November 26 and December 22, 1960 and were intended only as an exploratory survey. Preliminary results of a recent new series of measurements were used in the present paper. A short account of the investigation was given by VAN DE HULST (1961).

The design of the receiver and feed and their installation in the Dwingeloo mirror were carried out by SEEGER with the invaluable assistance of Drs K. J. VAN DAMME and Mr J. H. KUYPERS. Messrs A. MEESTER and W. VAN RIET were chiefly responsible for the successful mechanical design and construction of the rotating feed assembly. Observations were planned by SEEGER and WESTERHOUT and performed with the assistance of BROUW and TINBERGEN. The latter two carried out most of the reduction and discussion under the direction of WESTERHOUT.

This work was a project of the Netherlands Foundation for Radio Astronomy and financially supported by grants from the Netherlands Organization for the Advancement of Pure Research (Z.W.O.).

Our particular thanks go to Professors J. H. OORT, H. C. VAN DE HULST, C. A. MULLER and L. WOLTJER for stimulating discussions. In addition we wish to thank the following individuals and groups for many contributions which cannot all be stated here: Dr R. G. CONWAY, for the elegant synchronous demodulator, adder and subtractor units built during his stay in Leiden; Prof. J. VELDKAMP, Mr G. N. TAYLOR, Mr R. S. ROGER, Dr J. R. SHAKESHAFT and Dr V. A. RAZIN, who generously put pre-publication data at our disposal; the personnel of the Dutch P.T.T. television relay tower in Smilde, for assistance in mounting a microwatt test transmitter on their tower; Prof. C. A. MULLER and his staff at the Dwingeloo Observatory, who helped with the installation and during many emergencies; and finally, the various post and telegraph departments in the Netherlands and neighbouring countries, who have so effectively established and maintained an interference-clear band at 408 ± 2 Mc/s. These observations would not have been possible before this band was protected.

In the following chapters we give an account of the principles of the antenna and receiver and describe the observational procedure, followed by a discussion of the antenna properties. The VAN ALLEN belts and the interplanetary medium are shown to be negligible as sources of polarized radiation, and the influence of interstellar and ionospheric Faraday rotation is calculated. In the last three chapters the results of the observations are described and discussed, and a comparison is made with previous observations.

2. *Principles of instrument and reduction*

The receiver was of the well known correlation type, in which the output is the product of the instantaneous amplitudes in two orthogonal directions (Figure 1). As shown below, this quantity is proportional to the intensity of the polarized radiation. This method, used in conjunction with rotation of the antennas, rejects unpolarized radiation and eliminates certain cross-coupling effects. Because of the alt-azimuth mounting of the Dwingeloo mirror, it was possible to track a celestial source with a varying relation between the instrumental coordinate system and the sky. At the same time, of course, the aspect of the antenna with respect to the ground would change, with consequent variation of the effects of ground radiation. Thus, one can observe instrumental and real effects in differing combinations, so that a separation may be possible.

The feed consisted of an accurately constructed cylindrical waveguide section (length 90 cm, width 63 cm) with two orthogonal dipole probes. It was mounted coaxially on the central telescope mast and

FIGURE 1

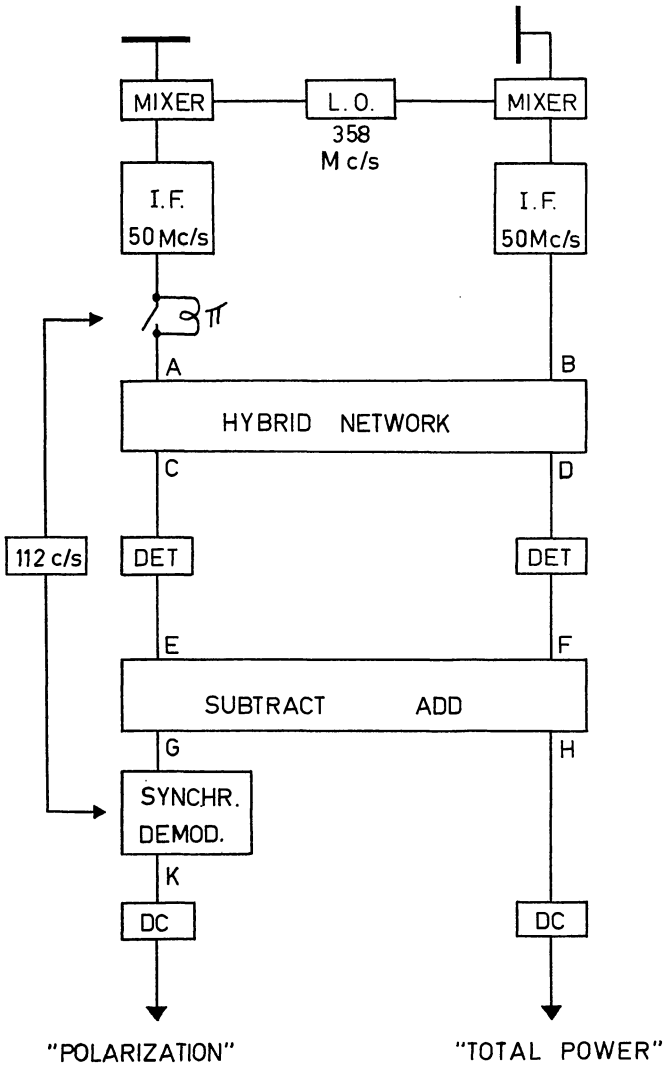

$E = C^2 = (B+A)^2$
$F = D^2 = (B-A)^2$
$G = E-F = 4BA$
$H = E+F = 2B^2+2A^2$
$K = \mp G = \mp 4BA$

Simplified block diagram of receiver showing voltages at various points.

was fitted with a flange to reduce spillover radiation. The advantages of such a feed are a high degree of symmetry and a low spillover fraction. The feed could be rotated by means of a small motor and set at eight different positions spaced at multiples of 45°. Rotary joints were incorporated in the two low-loss cables connecting the probes with the receiver.

A block diagram of the principal parts of the receiver is shown in Figure 1. The 408 Mc/s signals were immediately converted to 50 Mc/s in crystal mixers; image rejection was incorporated. The I. F. amplifiers were developed for low noise and good stability and were carefully adjusted to be closely equal in bandwidth, bandshape, gain and delay time. The bandwidths were 1.9 Mc/s. The phase-switch and synchronous demodulator were added to improve stability. The noise figure of the receiver as a whole was 3.8 (5.8 db). The attenuation between the probes and the mixers was 0.8 db.

The relations between various voltages occurring within the receiver are shown in Figure 1. If we receive both a linearly polarized signal and a randomly polarized one, the voltages A and B, in the absence of receiver noise, are

$$A = \pm\left\{e_0 \sin(\omega t+\alpha_0)\cos\eta_0 + e_1 \sin(\omega t+\alpha_1)\cos\eta_1\right\},$$
$$B = \quad e_0 \sin(\omega t+\alpha_0)\sin\eta_0 + e_1 \sin(\omega t+\alpha_1)\sin\eta_1,$$

where e_0, α_0, η_0 are respectively the amplitude, phase, and position angle of the plane of vibration (measured anti-clockwise from the direction of probe 1 in the feed) of the electric vector of the linearly polarized component, while e_1, α_1, η_1 are the corresponding quantities for the randomly polarized component. (Note that η_0 is fixed, while e_0, e_1, α_0, α_1 and η_1 vary randomly with time.)

We obtain the following results:

a) $$K = \mp 4BA = -4e_0^2 \sin^2(\omega t+\alpha_0)\sin\eta_0\cos\eta_0 + \text{terms in } \cos\eta_1 \text{ and/or } \sin\eta_1.$$

After smoothing by the output circuit, the "polarization" output is proportional to

$$-\frac{\overline{e_0^2}}{2}\sin 2\eta_0 = -I_0 \sin 2\eta_0.$$

b) $$H = 2B^2+2A^2 = 2e_0^2\sin^2(\omega t+\alpha_0)(\cos^2\eta_0+\sin^2\eta_0) + 2e_1^2\sin^2(\omega t+\alpha_1)(\cos^2\eta_1+\sin^2\eta_1) + \text{terms in } \cos\eta_1 \text{ or } \sin\eta_1.$$

After smoothing, the "total power" output is proportional to

$$\frac{\overline{e_0^2}+\overline{e_1^2}}{2} = I_0 + I_1.$$

The degree of polarization

$$P = \frac{I_0}{I_0+I_1} = \frac{I_0}{\text{"Total Power"}} = \frac{I_0}{I_T}$$

is the fraction of the power received in the form of linearly polarized radiation. This definition is equivalent to the more common one of

$$P = \frac{I_{\parallel}-I_{\perp}}{I_{\parallel}+I_{\perp}},$$

FIGURE 2

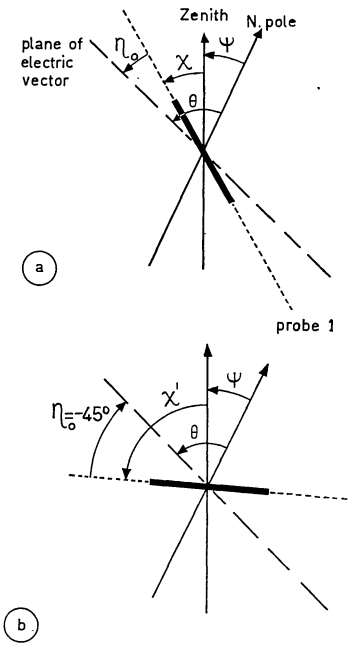

Relations between various position angles. a. Arbitrary position. b. Position of maximum output.

in which $I_{\parallel}$ = intensity of the radiation accepted by an antenna in the plane of maximum intensity,

$I_{\perp}$ = intensity of the radiation accepted by an antenna perpendicular to the plane of maximum intensity.

Receiver noise and direct coupling between the probes add an extra term to the polarization output which is independent of the position of the feed and is thus eliminated in our reduction. Coupling via the mirror or guy wires will, however, introduce terms which do depend on the feed position and give rise to at least part of the instrumental error discussed below.

When the feed is rotated, the polarization output will vary sinusoidally with a period of 180° in η_0, maximum positive amplitude being reached at $\eta_0 = 135°$ (and 315°). The position angle of probe 1 at this maximum, relative to the direction to the zenith, is converted into that of the plane of vibration of the electric vector, relative to the direction to the celestial North pole. Figure 2a shows probe 1 in a general position and indicates the relation between various angles of interest, as a projection on the celestial sphere along the telescope axis. The angle ψ is the position angle of the direction to the zenith, measured from the direction to the celestial North pole (also called the parallactic angle); the angle χ is the position angle of probe 1, measured from the direction to the zenith; the angle θ is the position angle of the plane of vibration of the incident electric vector, measured from the direction to the North pole. All angles increase anti-clockwise. We measure χ, but want θ, and they are related by

$$\theta = \eta_0 + \chi + \psi .$$

As the feed is rotated, the polarization output has a maximum at $\eta_0 = -45°$ (or $+135°$) (Figure 2b). If χ' is the value of χ at this maximum output, then

$$\theta = \chi' + \psi - 45° .$$

We can represent the $-I_0 \sin 2\eta_0$ curve by a vector of modulus I_0 and argument $2\eta_0$. This vector rotates with the feed, but twice as fast. The vector $\{I_0, 2(\chi' - 45°)\}$ rotates as time changes, while the vector $(I_0, 2\theta)$ is a property of the point of the sky under observation.

For further conversion to the galactic system of coordinates, we compute $\theta_{gal} = \theta + \varphi$, where φ is the galactic parallactic angle, the position angle of the direction to the equatorial North pole, from the direction to the galactic North pole. ψ and φ are taken from tables calculated at the Leiden Observatory.

The measurements were made at 8 fixed positions of the feed, separated by multiples of 45°. At the polarization output this yields two equivalent sets of four points on the $-I_0 \sin 2\eta_0$ curve (Figure 3). An overlay of standard sine curves was used to measure I_0 and $\chi' - 45°$. Intensity is measured in terms of an arbitrary unit and can be converted into brightness temperature with the aid of observations of standard sources, as described in Chapter 4. One unit corresponds to a polarization full-beam brightness temperature $\overline{T_b^p} = 0.40$ °K.

FIGURE 3

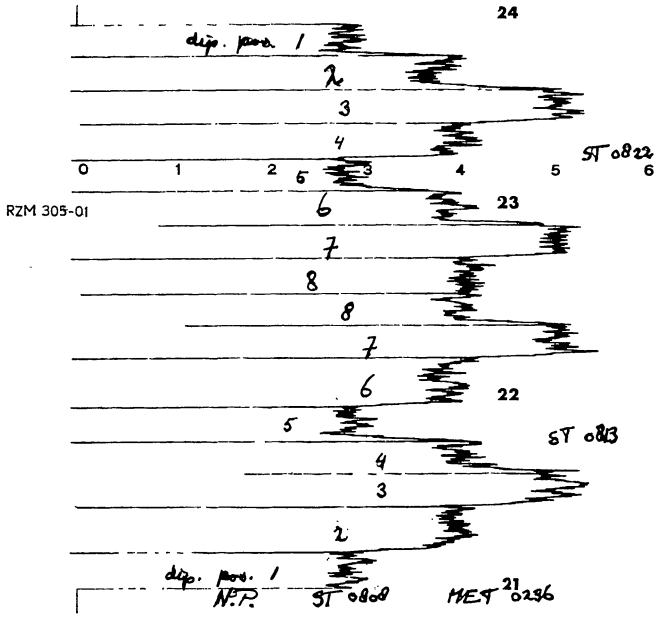

Sample measurement; $I_0 = 12$ units (instrument plus North pole). Numbers 1 to 8 denote probe positions.

3. *Measurements, reductions, and errors*

Since the stability of the instrument could not be counted on, a control measurement was made at the equatorial North pole every few hours, or even more often. The apparent values of I_o and $\chi' - 45°$ for these measurements, still influenced by instrumental effects, were each plotted against sidereal time. Figure 4 shows a series of histograms of the distribution of all North pole measurements, each histogram for an interval of one hour.

If no polarized signal had entered the antenna beam, and if the "zero error" (a vector quantity) had been constant throughout the whole period, the points would define a horizontal line. If, now, a weak polarized signal, whose magnitude was appreciably less than that of the zero error, was received, the points would have defined roughly sinusoidal curves which, on a polar plot, would form an off-centre circle (see Figure 5). In the actual histograms the maxima of the

FIGURE 4

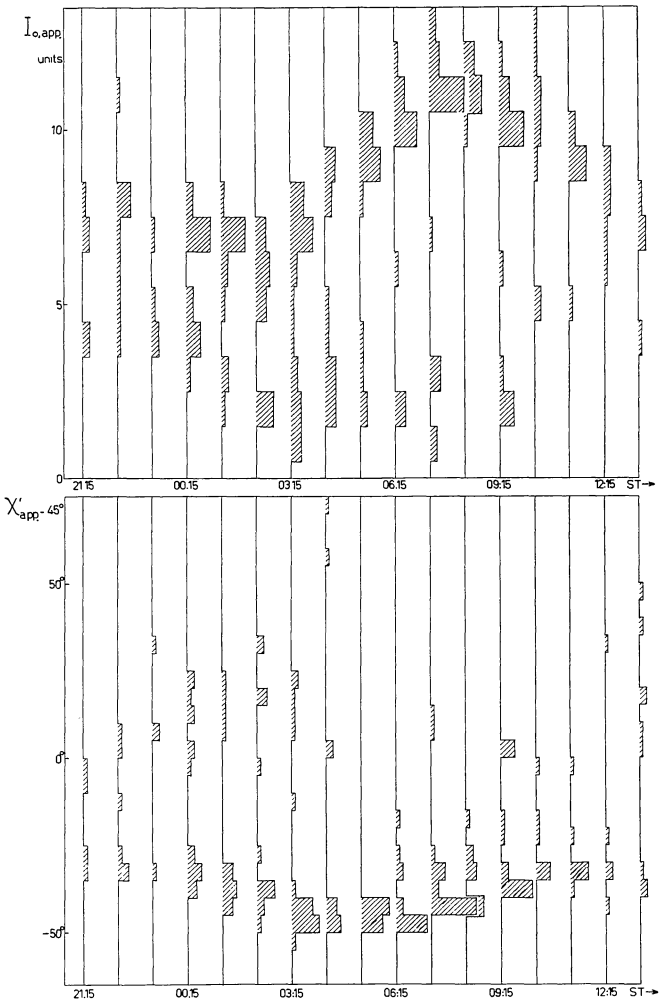

Histograms of apparent intensity and polarization angle observed at the North pole, in one-hour intervals.

FIGURE 5

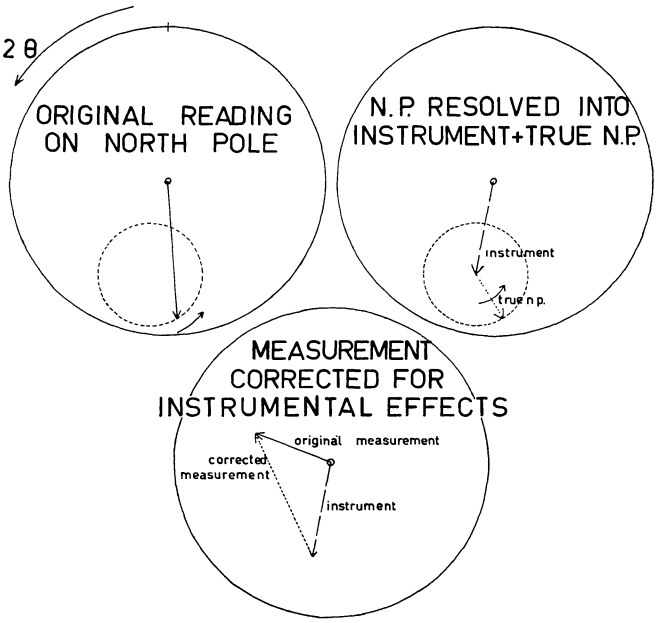

Separation of observed into instrumental and true polarization vectors.

distributions define just such a circle, though about one third of all the points lie well away from the maxima. This suggests that the zero error was constant most of the time, and was equal to the vector represented by the centre of the circle. Figure 6 shows measured North pole vectors for the two nights during which the instrument showed most and least variation. The true North pole vector is represented by the radius vector (for that particular sidereal time) of the circle; on this hypothesis we can deduce the zero error at any time from a North pole measurement. Measurements at other points made on the same day, at about the same time, can then be corrected for this zero error.

To test this hypothesis, the above procedure was carried out on six series of measurements at declination + 64°, all six overlapping over about 20° of right ascension. Figure 7 shows that the consistency of the data is considerably improved, thus justifying the interpretation.

After all our measurements had been corrected for the zero error, and the position angle had been transformed to the equatorial coordinate system, a few strange features still remained. A few of our observations of the same points, measured at the same elevation, but at different azimuths, showed a systematic difference. Furthermore, series of observations, made at the same elevation and azimuth, gave a polarization angle which was apparently constant over large regions of the sky.

During a new series of observations in October 1961 with an improved receiver, spurious polarized radia-

FIGURE 6

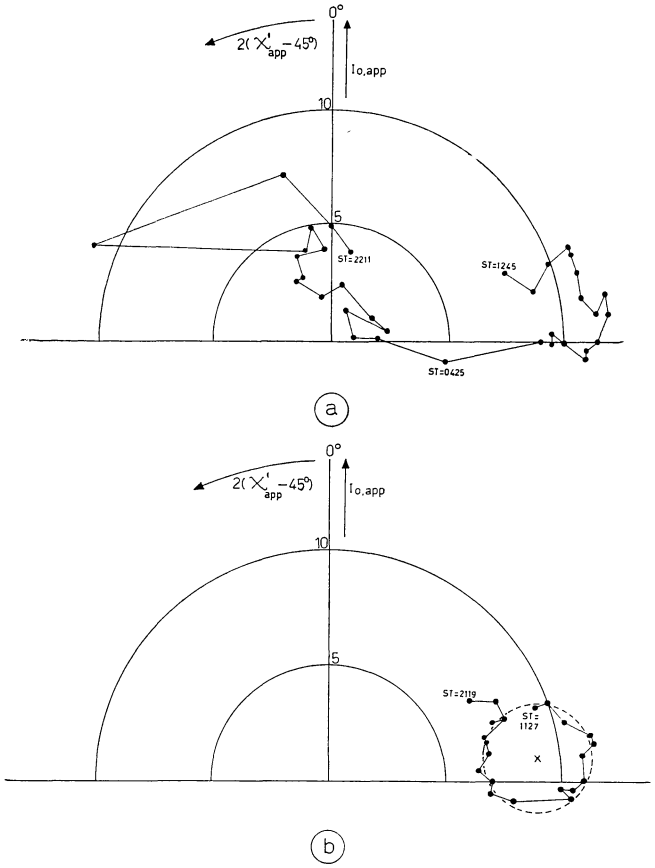

Measured North pole vectors on nights with most and least instrumental variation.

tion was detected. It was mainly vertically polarized and varied with elevation only. A preliminary curve, showing the relation between the intensity of this vertically polarized radiation and elevation is drawn in Figure 8.

Since the feed used in 1961 was not identical with that of 1960, it was not possible to use this curve to correct the present measurements. Not having obtained directly a similar relation for the present measurements, we could only get a very rough estimate of this spurious polarized radiation by taking at each elevation the average value of the polarization measurements. If the polarization of the background is completely random, this average value should represent the spurious polarization at that particular elevation. These average values had a vertical component only, which varied with elevation in the same way as in the new measurements (see Figure 8). Our observations were corrected for the "zero error" at the North pole, consisting of an instrumental zero error and the spurious polarized radiation at an elevation of 53° (the elevation of the North pole at Dwingeloo). If this is taken into account, the two curves in Figure 8 coincide below elevation 50°.

FIGURE 7

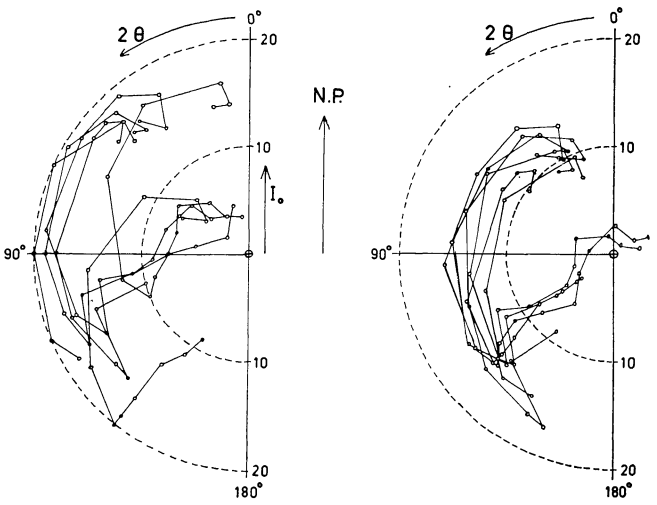

Effect of correction for instrumental variation on measurements at declination + 64°, right ascension 46° to 64°/86°.

Since we did not have any long enough series of observations at elevations above 50°, it was impossible to derive that part of the spurious polarization curve in the same way. The six series of measurements at declination + 64°, which were made at five different elevations above 50°, could not be brought together further by assuming a simple relation between spurious polarization and elevation above 50° such as the 1961 relation. We therefore assumed that the intensity of the spurious radiation is the same as at elevation 53°.

FIGURE 8

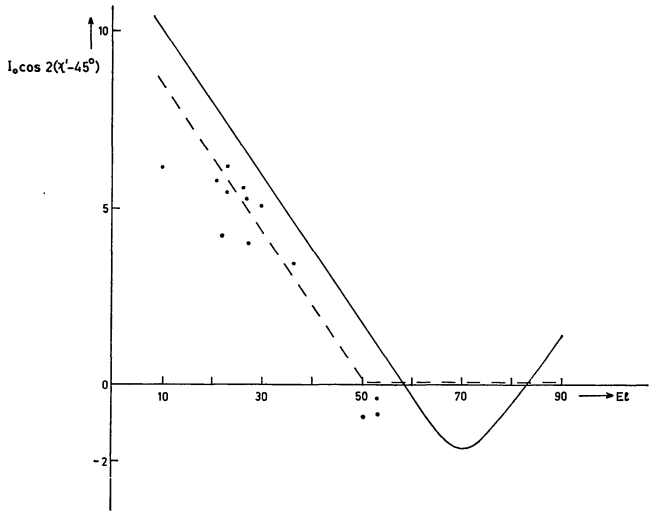

The intensity of the vertically polarized spurious radiation as a function of elevation. Negative values denote horizontal polarization. The component $I_o \sin 2(\chi' - 45)$ was almost zero. The full line represents the 1961 relation. The 1960 observations are shown as dots, and the broken line is the relation adopted for 1960.

FIGURE 9

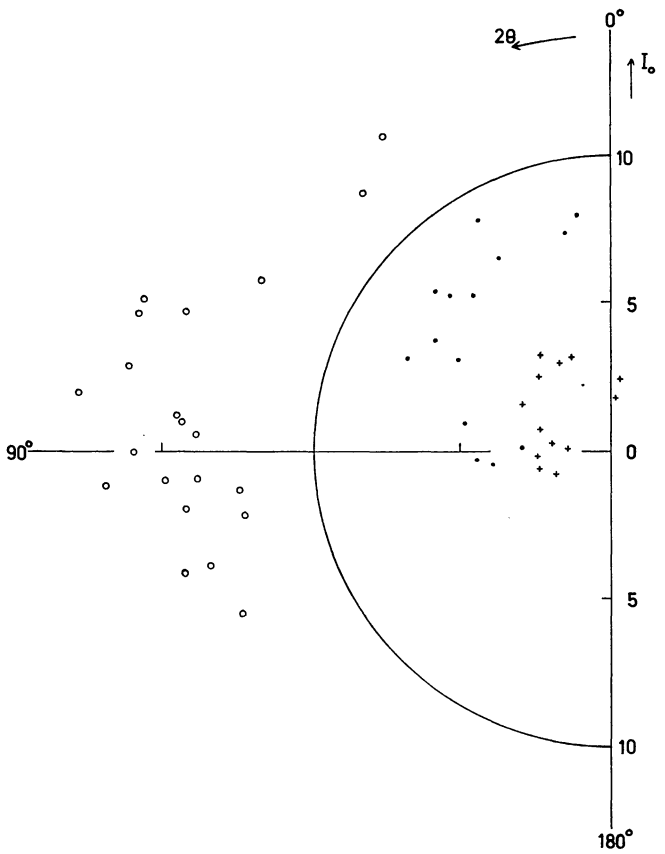

Individual observations of the points $\alpha = 340°$, $\delta = +58°.5$ (· before, + after correction for spurious polarized radiation) and $\alpha = 57°$, $\delta = +64°$ (∘ ; for this point the correction is zero).

Figure 9 and Table 1 show all the observations of the point $\alpha = 340°$, $\delta = +58°.5$, which was measured at several different elevations below 50°, with and without the correction for spurious radiation. The consistency of the corrected values is much better, which is a justification of the correction process. The measurements at the point $\alpha = 57°$, $\delta = +64°$ are also given; since they were all made above elevation 50°, no correction for spurious radiation was applied.

Routine reduction therefore consisted of the following steps:

a) Deduce the variation of the zero error during each night from the North pole measurements.

b) Using interpolated zero-error values where necessary, correct the apparent values of I_o and $\chi' - 45°$ by vectorially subtracting the zero error.

c) Subtract the spurious polarization vector for the elevation at which the measurement was made.

d) Add ψ to the corrected values of $\chi' - 45°$ to obtain θ.

e) Collect all observations at the same right ascension and declination, and calculate I_o and θ corresponding to the centre of gravity of the points representing the vectors.

f) Add φ to θ to obtain θ_{gal}.

The mean errors $\left(\sqrt{\frac{\sum\Delta^2}{n-1}}\right)$ in the orthogonal components of the polarization vector $(I_o, 2\theta)$ for one measurement, derived for all the points which were measured more than once, is $\pm$ 2.2 units. Hence the mean errors ΔI_o in the intensity, and $\Delta\theta$ in the polarization angle can be represented by:

$$\Delta I_o = \pm 2.2 \text{ units},$$

$$\Delta\theta = \pm \frac{63}{I_o} \text{ degrees}.$$

The points which were measured ten times or more are listed in Table 2, together with the mean error in their average intensities and polarization angles.

TABLE 1

Observations with and without correction for spurious polarized radiation.

δ	α	El	uncorrected		corrected	
			I_o (units)	θ	I_o (units)	θ
58°.5	340°	23°	8.0	4°	2.5	176°
		23	7.5	6	2.0	178
		25	7.5	15	2.5	37
		25	9.0	15	3.5	11
		29	8.0	24	4.0	18
		30	7.5	23	3.5	15
		31	7.5	33	3.5	32
		31	6.0	30	2.0	42
		32	7.0	29	3.5	22
		33	7.0	21	4.5	8
		33	5.0	40	2.5	47
		37	4.5	47	2.0	56
		42	4.0	49	2.5	52
		44	3.0	44	1.5	44
64	57	52	12.0	22		
		52	13.0	18		
		52	13.0	38		
		53	14.5	43		
		53	14.0	44		
		56	14.0	53		
		62	13.5	57		
		62	13.0	32		
		63	15.0	53		
		63	12.5	50		
		64	12.5	48		
		69	15.0	47		
		71	14.5	43		
		74	16.5	40		
		75	18.0	42		
		75	16.5	36		
		76	16.5	37		
		78	15.0	36		
		78	14.5	49		
		78	16.0	45		
		78	17.0	47		
		79	14.0	47		

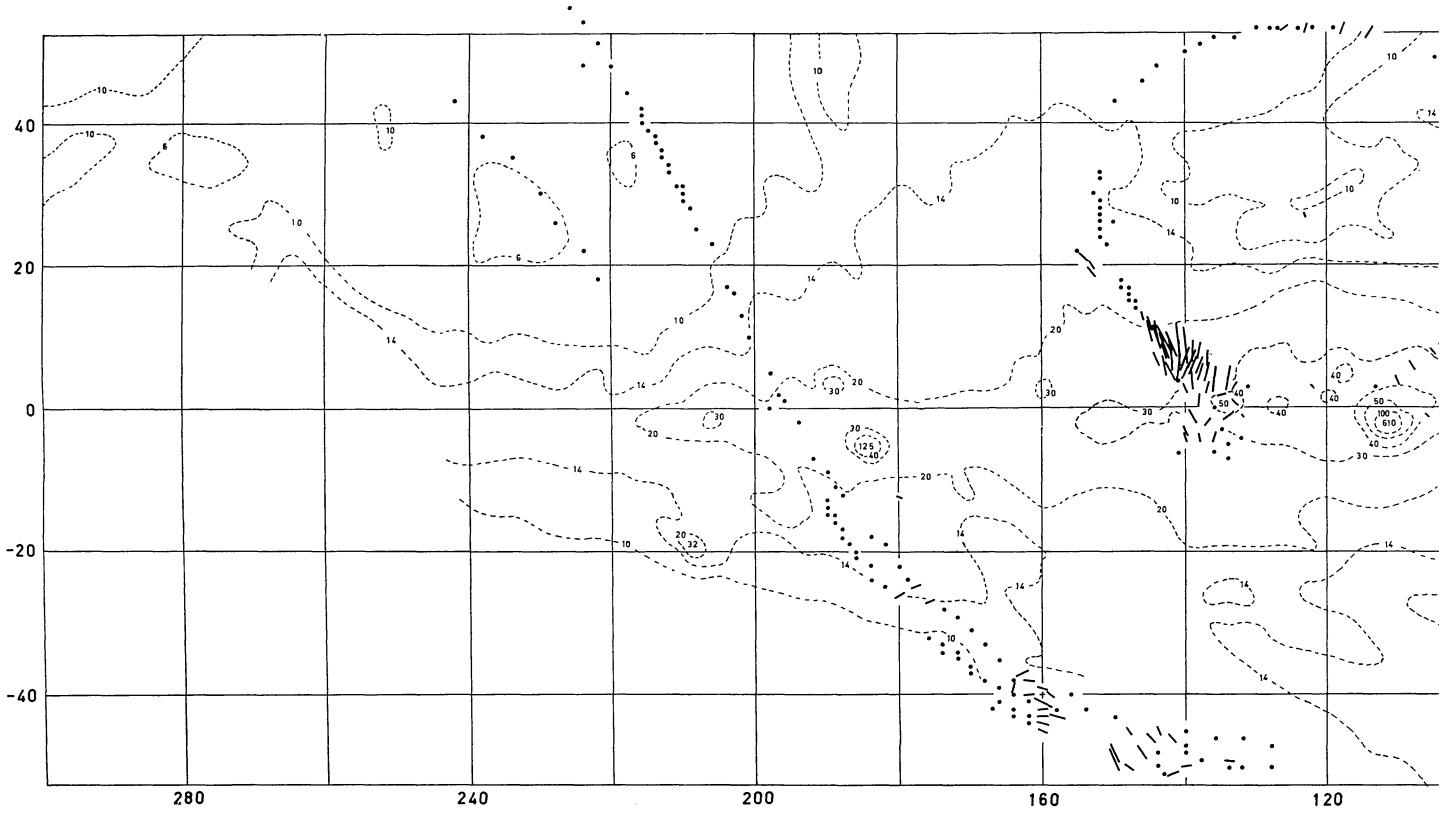

a

b

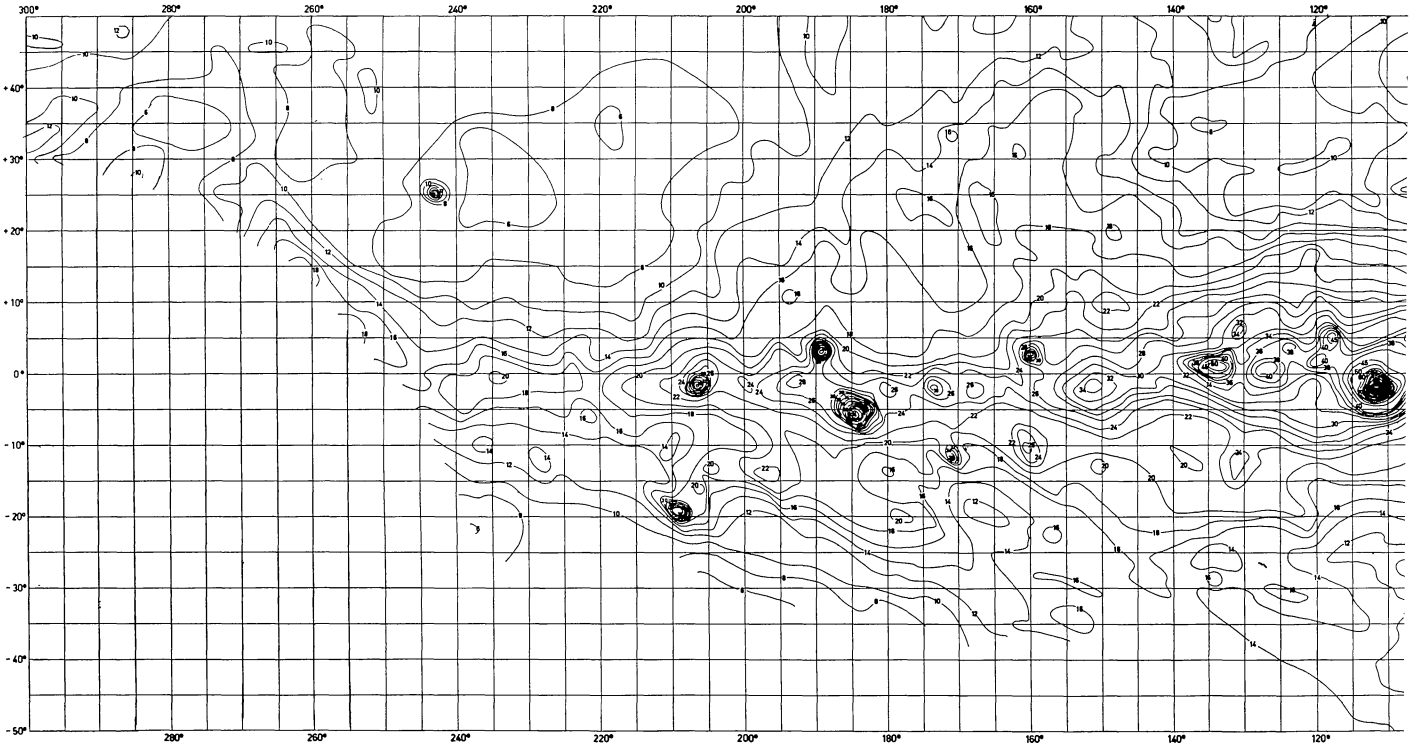

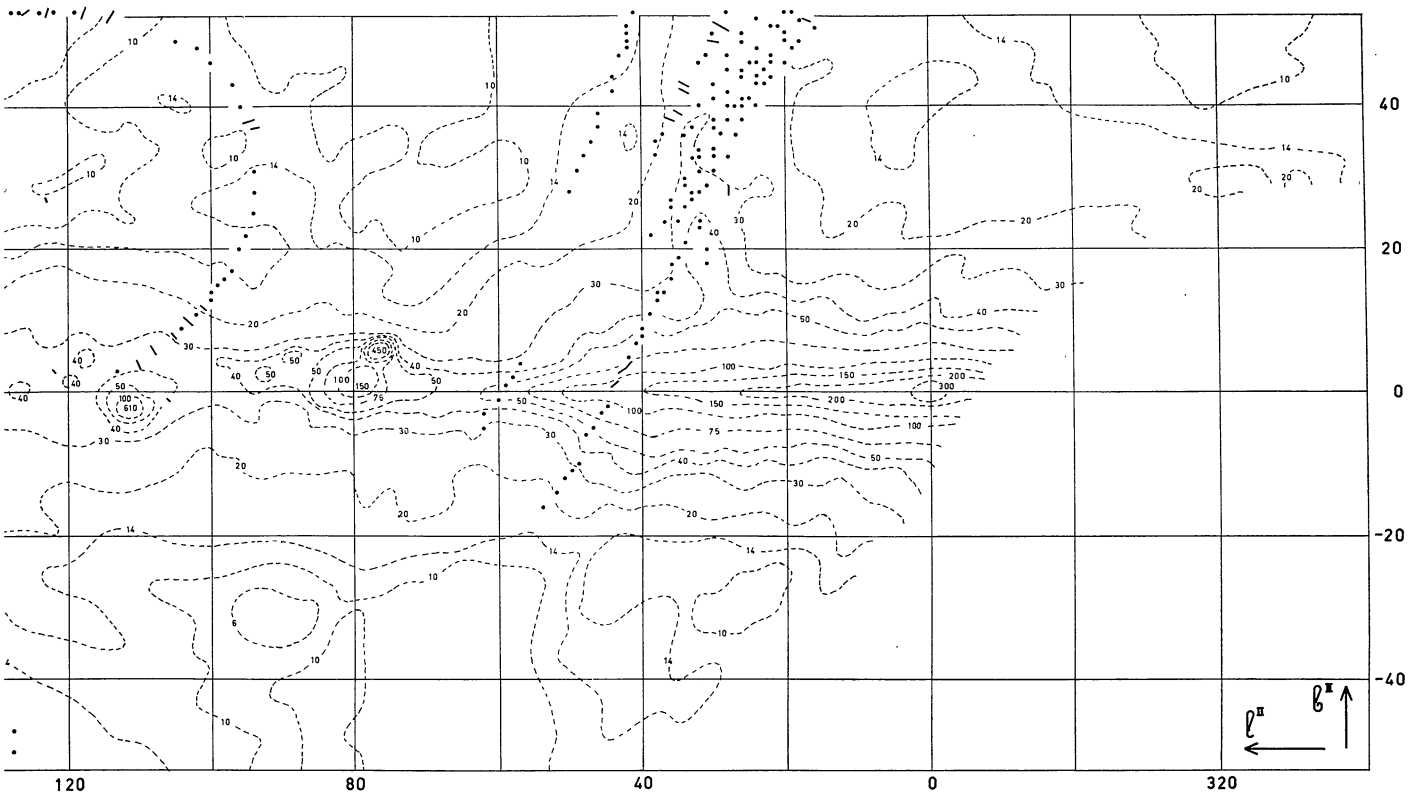

a. Polarization measurements plotted on simplified contour maps of 75-cm unpolarized background radiation. The length of the lines represents the intensity I_o, the direction represents the galactic position angle θ_{gal} of the electric vector.

b. Complete contour maps. $\overline{T}_b = (13 + 1.2 \times \text{contour units})$ °K.

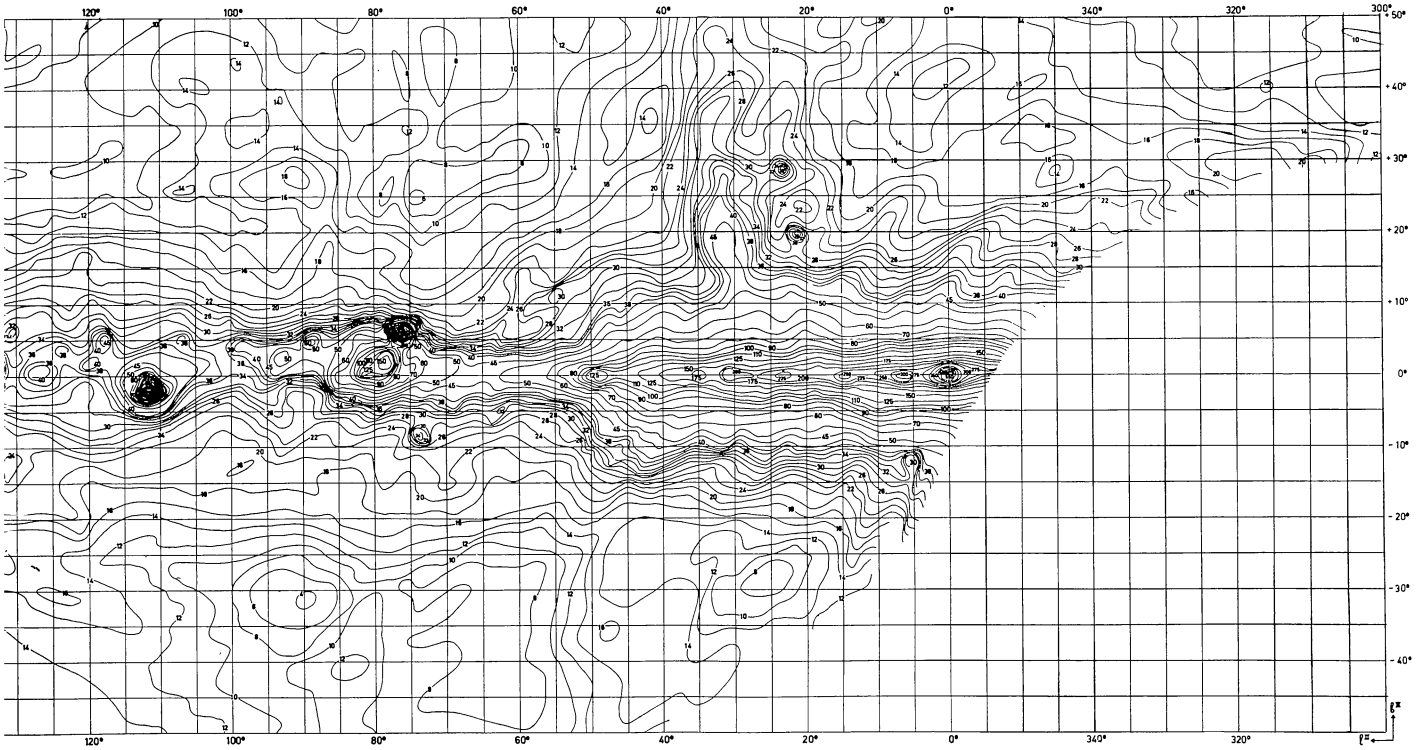

FIGURE 10

a.

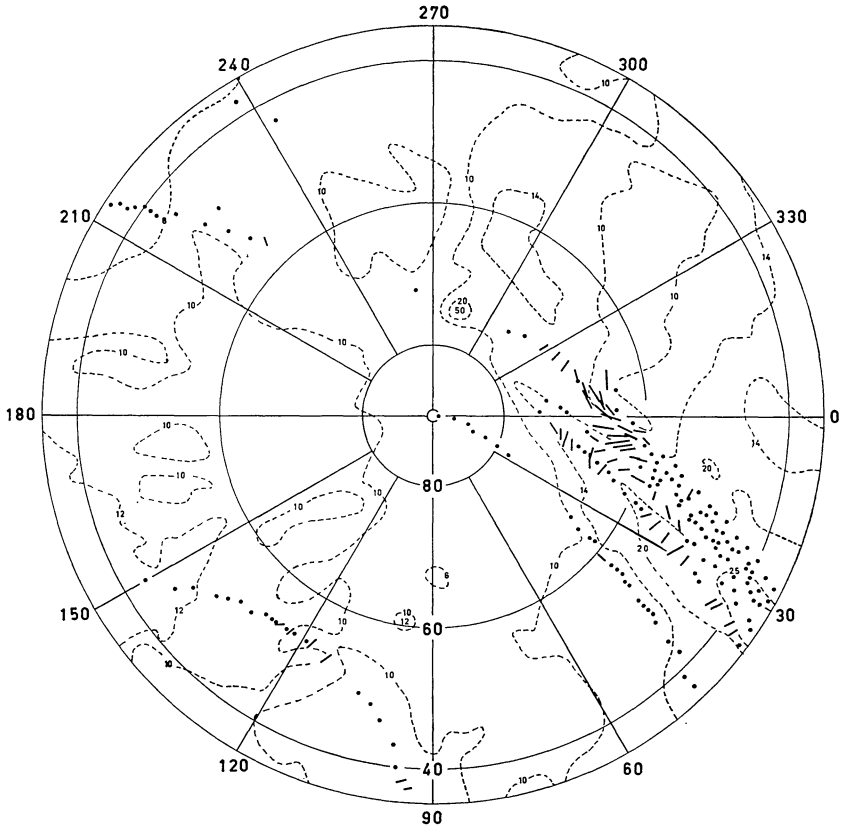

I =10 units
=4 °K

b.

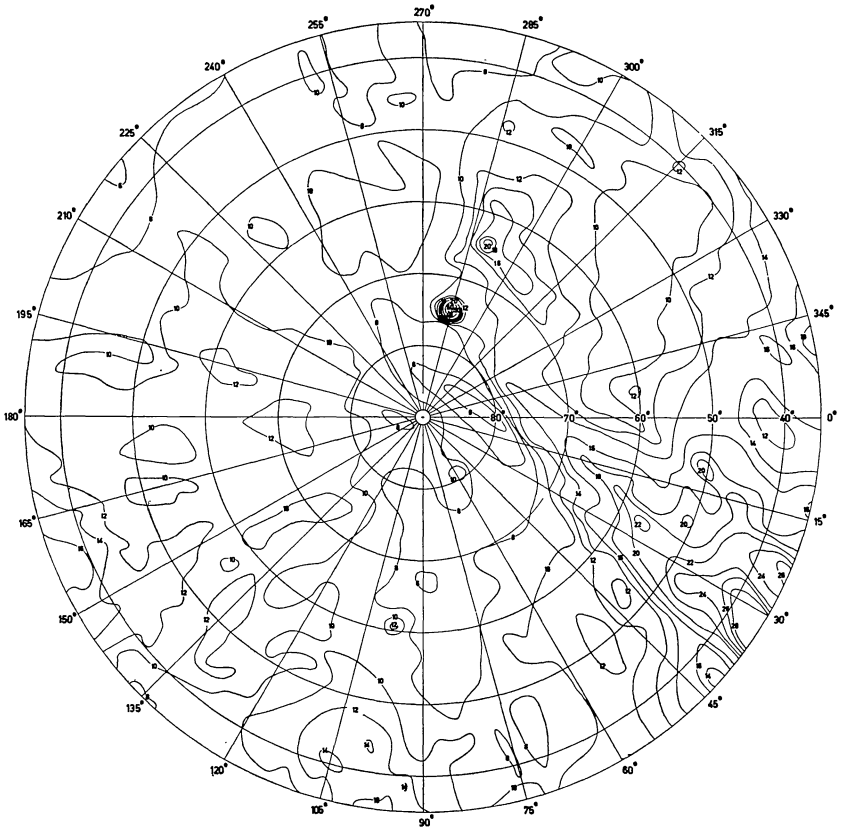

TABLE 2

Intensities and polarization angles measured ten times or more.

δ	α	n	$\bar{I}_o$	m. e.	$\bar{\theta}$	m. e.
+13°	38°	20	8.7	±0.6 units	106°	± 2°
+13	180	12	1.1	0.8	103	20
+22	75	10	2.5	1.3	63	14
+58.5	340	15	2.0	0.5	24	7
+61	30	19	1.5	0.7	55	13
+64	57	22	14.0	0.6	42	2
+65.5	12	17	3.0	0.5	39	22

Little is known about systematic errors. The considerations in Chapter 7 lead to an estimate of a systematic error in the polarization angle θ, due to ionospheric Faraday rotation. Since most of our observations were made in a part of the sky where the longitudinal component of the earth's magnetic field is towards the observer, this error is indeed a systematic one in the sense that the observed value of θ is greater than the value outside the earth's ionosphere. The error is of the order of + 20° in θ.

Table 3 gives a summary of the results for all the observed points with a measured intensity ≥ 5 units, and for all other points which were measured ten times or more. A total of 503 points was measured. The 157 points given in Table 3 are the only results in which we have some confidence. The equatorial coordinates are accurate to ½° only. Since the conversion to galactic coordinates was done to the nearest degree, these may be in error by 1° in either coordinate. The old galactic pole was used in the calculation of φ, the galactic parallactic angle.

Numbers in the "Remarks" column refer to the list below the table. Due to the proximity of a point source (sources taken from DAVIS *et al.* 1962), the true value of the polarization vector ($\bar{I}_o$, 2 $\bar{\theta}$) may lie anywhere within a circle centred on the point ($\bar{I}_{o,\,observed}$, 2 $\bar{\theta}_{observed}$). The radius of this circle is given for each point where this error was greater than 1 unit.

The value of $\bar{I}_o$ for the North pole was taken from the histograms of observed I_o. The value of $\bar{\theta}_{gal}$ for the North pole was derived from Figure 14; note that the North pole value thus is the only value which is corrected for the ionospheric Faraday rotation.

In Figure 10 the observations are plotted as lines centred on the position of the observed point, on maps of the continuous background radiation at 75 cm, measured at Dwingeloo in 1957 (SEEGER *et al.* 1962). The length and direction of each line correspond to $\bar{I}_o$ and $\bar{\theta}_{gal}$. The dots indicate measured points which are not included in Table 3.

The units on the contour maps are 1.2 °K of full-beam brightness temperature. The zero level is unknown; recent measurements at the Mullard Radio Astronomy Observatory, Cambridge (*private communication*) showed that the North pole has $\overline{T_b} = 25$ °K at 408 Mc/s, indicating that the zero level underlying the continuum maps is about 11 units, or 13 °K in $\overline{T_b}$. Therefore, the brightness temperature of the unpolarized 75-cm background radiation is $\overline{T_b} = (13 + 1.2 \times$ units of contour map) °K. In addition to the uncertainty in the zero level, a further uncertainty in $\overline{T_b}$ arises from the fact that the existence of so strong a polarized component was not realized at the time the maps were made.

TABLE 3

Intensities and position angles of the polarized radiation at all points where we have some confidence in the measurements. 1 unit = 0.4 °K in $\overline{T_b^p}$.

δ_{1950}	α_{1950}	l^{I}	b^{I}	l^{II}	b^{II}	n	I_o (units)	θ	θ_{gal}	Remarks
+ 8°	255°	355°	+26°	28°	+28°	2	5.0	117°	0°	
+ 9	210	318	+63	348	+65	1	11.0	24	80	
+ 9.5	24	111	−49	142	−51	2	7.0	130	111	
	28	117	−48	148	−50	2	6.5	80	56	
	30	120	−47	150	−49	2	13.0	50	23	
	38	129	−43	160	−45	2	6.0	100	65	
+10	283	10	+ 2	42	+ 4	1	5.5	76	138	
	285	11	0	43	+ 3	1	5.0	61	123	
	286	12	− 1	44	+ 1	1	5.5	69	130	
+11	24	111	−49	140	−50	2	5.5	117	98	
	28	117	−47	146	−48	2	9.0	59	35	
	30	119	−46	150	−48	2	11.0	49	23	
	38	129	−43	160	−44	2	7.0	110	76	
	200	301	+70	328	+72	1	5.0	153	0	
	202	306	+69	333	+71	1	6.5	168	20	

TABLE 3 (*continued*)

δ_{1950}	α_{1950}	l^{I}	b^{I}	l^{II}	b^{II}	n	I_o (units)	θ	θ_{gal}	Remarks
+11°	204°	310°	+68°	339°	+70°	1	7.0	177°	33°	
	206	314	+67	344	+69	1	6.5	50	89	
	209	320	+65	350	+68	2	9.5	54	98	
	210	321	+64	352	+67	1	11.0	70	115	
	211	323	+64	354	+66	1	9.0	53	99	
	212	325	+63	356	+66	3	6.5	62	109	
	213	326	+62	358	+65	1	7.5	77	125	
	218	332	+59	4	+61	2	6.5	123	176	
+12.5	210	324	+66	354	+68	1	11.5	66	113	
	212	327	+64	358	+66	1	12.5	87	137	
	214	330	+63	0	+65	1	12.0	109	161	
	216	332	+61	4	+63	2	9.0	105	158	
	218	335	+60	6	+62	2	7.5	108	163	
	220	337	+58	8	+60	1	5.5	87	143	
	229	345	+50	17	+52	1	5.0	8	69	
+13	20	105	−48	134	−49	1	6.5	99	86	
	38	127	−41	158	−43	20	8.5	106	73	
	39	128	−40	160	−43	1	5.5	125	91	
	40	129	−40	160	−42	1	6.0	132	97	
	44	133	−37	164	−39	1	6.0	23	164	
	63	149	−24	180	−26	1	6.0	171	120	
	180	234	+72	262	+72	12	1.0	103	73	1
+14	26	112	−45	142	−46	2	5.5	62	42	
	28	115	−45	145	−46	2	7.0	67	45	
	30	117	−44	148	−45	2	5.0	60	35	
	40	129	−39	160	−41	2	11.0	98	63	
	42	131	−38	162	−40	2	6.5	131	95	
	214	332	+64	4	+66	1	11.5	120	174	
	216	335	+62	6	+64	1	12.0	128	4	
	217	336	+61	8	+64	1	14.0	141	18	
	218	337	+60	9	+63	1	11.0	139	16	
	219	338	+60	10	+62	1	8.5	136	14	
	220	339	+59	12	+61	1	6.5	125	4	
	221	340	+58	12	+60	1	6.5	119	178	
+15.5	28	114	−43	144	−45	2	6.5	45	23	
	40	127	−38	159	−40	1	5.5	87	53	
	41	128	−37	160	−39	1	5.5	108	73	
	43	130	−36	162	−38	1	6.5	118	82	
	45	132	−35	163	−37	1	7.5	153	115	
	60	144	−25	176	−27	1	5.5	160	112	
	63	146	−23	178	−25	1	5.5	160	110	
	158	196	+58	226	+56	1	5.0	38	155	
+16	214	336	+65	8	+67	1	5.5	99	156	
	216	338	+63	12	+66	1	6.0	143	22	
	218	341	+61	14	+64	1	5.5	152	32	
	220	343	+60	16	+62	1	6.0	137	18	
	222	344	+58	17	+60	1	8.5	107	169	
	226	347	+55	20	+57	1	5.0	31	95	
	229	350	+52	22	+54	1	7.5	63	128	
	231	351	+50	24	+52	1	6.5	60	125	
+18.5	208	333	+71	6	+73	1	7.0	71	128	
	210	336	+69	8	+72	1	5.5	44	103	
	211	338	+68	10	+71	1	9.0	22	82	
	212	339	+68	12	+70	1	6.0	39	100	
	215	343	+65	14	+67	2	6.5	24	87	
	216	344	+64	16	+67	1	8.5	43	106	
	218	345	+63	18	+65	1	7.5	1	65	

TABLE 3 (*continued*)

δ_{1950}	α_{1950}	l^{I}	b^{I}	l^{II}	b^{II}	n	$I_{\circ}$ (units)	θ	θ_{gal}	Remarks
+18°.5	227°	352°	+55°	25°	+57°	2	5.5	153°	40°	
	229	353	+53	26	+55	2	8.0	177	65	
	231	355	+51	28	+53	2	7.0	12	80	
	233	356	+50	29	+51	1	9.5	171	59	
	236	357	+47	30	+49	1	7.0	11	79	
	242	0	+42	34	+43	1	7.0	173	62	
	244	1	+40	34	+42	1	7.0	173	62	
	246	2	+38	35	+39	1	5.5	173	61	
	248	3	+36	36	+38	1	5.5	1	69	
+22	75	148	−10	180	−12	10	2.5	117	63	2
+26	227	5	+57	40	+59	1	5.0	100	178	
+54	43	109	− 3	140	− 4	1	5.5	46	17	
+56	35	104	− 3	136	− 4	1	6.0	5	163	
	39	106	− 2	138	− 4	1	5.0	35	10	
	43	108	− 1	140	− 3	1	5.5	57	28	
+58	39	105	− 1	137	− 2	1	5.0	169	144	
	43	107	0	139	− 1	1	8.0	57	28	
+58.5	340	74	0	106	− 1	15	2.0	24	50	3
+60	31	100	0	132	− 1	1	8.5	150	132	
	25	102	0	134	− 1	1	7.5	146	124	
	43	106	+ 2	138	+ 1	1	7.5	22	173	
+61	30	100	0	132	− 1	19	1.5	55	37	
	48	107	+ 4	140	+ 3	2	5.5	58	25	
	54	109	+ 6	142	+ 5	2	11.5	67	29	
	57	110	+ 7	143	+ 6	2	11.5	52	11	
	60	112	+ 7	144	+ 7	2	8.0	67	24	
	91	120	+20	153	+19	1	7.0	107	39	
	93	121	+20	153	+20	1	6.0	102	32	
	94	121	+21	154	+21	1	7.0	118	47	
+62	35	101	+ 2	133	+ 1	1	5.5	72	50	4
	39	103	+ 3	135	+ 2	1	5.0	129	104	5
	43	105	+ 4	137	+ 3	1	7.0	16	167	
+62.5	48	107	+ 5	139	+ 4	2	11.5	38	5	
	51	108	+ 6	140	+ 5	2	9.0	12	156	
	54	109	+ 7	141	+ 6	2	15.0	32	174	
	57	110	+ 8	142	+ 7	2	12.0	45	4	
	60	111	+ 9	143	+ 8	2	9.0	58	15	
+64	31	99	+ 4	131	+ 3	1	5.0	163	145	
	39	102	+ 5	134	+ 4	1	13.5	15	170	
	43	104	+ 6	136	+ 4	1	13.5	22	173	
	46	105	+ 6	137	+ 5	3	10.5	18	167	
	47	105	+ 6	138	+ 5	3	9.5	15	163	
	48	105	+ 7	138	+ 6	3	10.5	10	157	
	49	106	+ 7	138	+ 6	3	9.5	14	160	
	50	107	+ 7	139	+ 6	1	10.0	13	158	
	51	107	+ 7	139	+ 6	6	12.0	12	156	
	52	107	+ 8	139	+ 7	1	11.0	14	157	
	53	108	+ 8	140	+ 7	1	13.0	17	160	
	54	108	+ 8	140	+ 7	6	14.0	23	165	
	55	108	+ 8	140	+ 7	1	13.0	32	154	
	56	108	+ 9	141	+ 8	2	13.5	28	168	
	57	109	+ 9	141	+ 8	22	14.0	42	1	

TABLE 3 (*continued*)

δ_{1950}	α_{1950}	l^{I}	b^{I}	l^{II}	b^{II}	n	$I_{\circ}$ (units)	θ	θ_{gal}	Remarks
+64°	58°	109°	+10°	142°	+ 8°	1	13.0	49°	7°	
	59	110	+10	142	+ 8	4	14.5	54	11	
	60	110	+10	142	+ 9	5	14.5	62	19	
	61	110	+11	142	+ 9	2	15.5	71	27	
	62	111	+11	143	+ 9	4	14.5	65	20	
	63	111	+11	143	+10	1	14.5	72	26	
	64	111	+12	143	+10	1	16.5	79	32	
	65	112	+12	144	+10	4	13.5	66	18	
	66	112	+12	144	+10	1	13.0	67	19	
	67	112	+12	144	+11	3	11.0	60	11	
	68	112	+13	145	+11	1	12.0	64	14	
	69	113	+13	145	+12	1	8.0	72	21	
	70	113	+13	145	+12	4	7.5	63	11	
	72	114	+14	146	+13	1	5.5	75	19	
	73	114	+14	146	+13	3	5.0	64	10	
	188	91	+54	126	+53	1	5.0	122	125	
	192	89	+54	123	+53	1	5.5	165	162	
	199	83	+54	118	+53	1	7.0	172	159	
	205	79	+53	114	+52	1	7.5	171	149	
	249	61	+39	95	+38	1	6.0	3	108	
	253	61	+37	94	+37	1	5.0	2	103	
	314	68	+12	101	+12	1	5.0	2	50	
	321	70	+10	103	+10	1	7.0	5	48	
	329	73	+ 8	105	+ 8	1	5.0	3	39	
	335	75	+ 6	108	+ 6	1	5.5	1	32	6
	342	78	+ 5	110	+ 4	1	5.5	178	23	
+65.5	12	91	+ 4	122	+ 3	17	3.0	39	38	
	48	105	+ 8	137	+ 7	2	8.5	30	177	
	51	106	+ 9	138	+ 8	2	9.5	26	170	
	54	107	+ 9	139	+ 8	2	12.0	31	174	
	57	108	+10	140	+ 9	2	19.5	46	5	
	60	109	+11	141	+10	2	17.0	50	6	
+90	—	90	+28	123	+27	90	2.4	—	22	7

Remarks: 1. Vir A comparison field.
2. Tau A comparison field.
3. Cas A comparison field.
4. Point source at $\delta = +61°.8$, $\alpha = 36°$. Possible error 3 units.
5. Point source at $\delta = +61°.8$, $\alpha = 36°$. Possible error 2 units.
6. Point source at $\delta = +63°.2$, $\alpha = 336°$. Possible error 1 unit.
7. North pole, value outside earth's atmosphere. Determination of I and θ differs from that at other points. See text.

4. *Antenna characteristics and calibration*

We shall now describe the calculation of some antenna characteristics and the calibration of the intensity scale. The definition of a number of terms used in this and other chapters follows below.

$f(\theta, \varphi)$: Antenna pattern, power response to a randomly polarized wave of the antenna in the direction (θ, φ) relative to the maximum response $f(0,0) = 1$.

Full beam: The part of the antenna pattern down to a level necessary for the problem under consideration. In this paper, the full beam contains the first side lobes out to about 7 degrees from the axis.

Ω: Antenna solid angle, integral of the antenna pattern over the sphere. $\Omega = \int_{4\pi} f(\theta, \varphi)\, d\Omega$.

Ω': Beam solid angle, integral of the antenna pattern over the full beam.

D: Directivity, ratio of maximum antenna power response to average power response over all directions. $D = 4\pi/\Omega$.

D': Beam directivity, ratio of maximum antenna power response to average power response over all directions if $f(\theta, \varphi)$ were zero outside the full beam. $D' = 4\pi/\Omega'$.

β: Stray factor, fraction of the total power which the antenna would absorb in an isotropic radiation field, incident from directions outside the full beam (diffraction side lobes, scattering against feed and feed supports, spillover, and radiation through the reflecting screen). $\beta = 1 - \Omega'/\Omega = 1 - D/D'$.

η_B: Beam efficiency, fraction of the total power, incident from the full beam, which is available at the antenna terminals. It includes a factor η_R, the radiation efficiency, which specifies the losses in the reflector surface and the feed. $\eta_B = (1 - \beta)\,\eta_R$.

T_b: Brightness temperature in a particular direction, temperature of a black body situated in that direction for which the brightness of the thermal radiation would equal the observed brightness, B. $T_b = \lambda^2 B/2k$.

$\overline{T}_b$: Full-beam brightness temperature, mean value of the brightness temperature over the full beam.

$$\overline{T}_b = \frac{1}{\Omega'} \int_{\text{full beam}} f(\theta, \varphi)\; T_b(\theta, \varphi)\, d\Omega .$$

T_A: Antenna temperature, absolute temperature of an impedance, identical to the antenna impedance which, if connected in place of the antenna, would deliver the same available noise power to the antenna terminals as the antenna.

$$T_A = \frac{\eta_R}{\Omega} \int_{\text{sphere}} f(\theta, \varphi)\; T_b(\theta, \varphi)\, d\Omega =$$

$$= \frac{\eta_B}{\Omega'} \left\{ \int_{\text{full beam}} f(\theta, \varphi)\; T_b(\theta, \varphi)\, d\Omega + \int_{\substack{\text{sphere} \\ -\text{full} \\ \text{beam}}} f(\theta, \varphi)\; T_b(\theta, \varphi)\, d\Omega \right\} .$$

If the last term is constant over a measurement, $T_A = \eta_B \overline{T}_b + \text{constant}$.

T_b^p: Polarization brightness temperature of a linearly polarized region in the sky, the difference between the brightness temperature measured with a linearly polarized antenna which receives all the polarized radiation, and a similar antenna at right-angles, which measures none. If one wanted to adhere to the classical definition of brightness temperature as the temperature of a black body (see above), this polarization brightness temperature may be described as the temperature of a black body shining through a linearly polarized screen (a "linearly polarized black body"), replacing the emitting region, and giving the same total flux at the antenna as the linearly polarized region.

T_A^p: Polarization antenna temperature, difference between the antenna temperature of a linearly polarized antenna which receives all the polarized radiation, and that of a similar antenna at right-angles, which receives none.

$I_{\parallel}$: Intensity of the radiation accepted by a linearly polarized antenna in the plane of maximum intensity. If T_b is the brightness temperature of the randomly polarized component, $I_{\parallel} \propto T_b + T_b^p$.

$I_{\perp}$: Intensity of the radiation accepted by a linearly polarized antenna perpendicular to the plane of maximum intensity. $I_{\perp} \propto T_b$.

P: Degree of polarization. $P = \dfrac{I_{\parallel} - I_{\perp}}{I_{\parallel} + I_{\perp}} = \dfrac{T_b^p}{2\,T_b + T_b^p}$.

The deflection of the total-power recorder I_T is proportional to $I_{\parallel} + I_{\perp}$ and thus $I_T \propto 2\; T_b + T_b^p$. This deflection was constant and equal to the amplitude I_o of the double sine curve in the deflection of the polarization recorder, obtained when the feed was rotated through 360° and the telescope was pointed at a high-intensity, linearly polarized test transmitter at a distance of 10 km. Since T_b was practically zero as compared to T_b^p, this experiment showed that the constants c in $I_o = c.\,T_b^p$ and $I_T = c.\,(2\,T_b + T_b^p)$ were equal. The value of c can be determined by measuring the deflection ΔI_T of the total-power recorder when the brightness temperature of unpolarized incoming radiation increases by ΔT_b, $\Delta I_T = c.2\,\Delta T_b$. We may calibrate in units of full-beam brightness temperature if we put $I_T = c.\,2\,\overline{T}_b$.

If we know the antenna temperature and the beam efficiency η_B we can calculate the full-beam brightness temperature of an unpolarized source or of unpolarized extended regions. The beam efficiency, however, is hard to calculate or to measure. If we are interested only in the full-beam brightness temperature, we do not need η_B if the flux density S of one point source is known. Equating this flux density to the deflection of the total-power recorder when the source passes the beam enables us to calculate the flux density S_u of a source giving a deflection of 1 unit (SEEGER *et al.* 1956). This deflection could also be caused by the flux received from an extended region with a full-beam brightness temperature $\overline{T}_{b,u}$,

$$S_u = \frac{2\,k\,\overline{T}_{b,u}\,\Omega'}{\lambda^2} = \frac{8\,\pi\,k}{D'\lambda^2}\,\overline{T}_{b,u} ,$$

from which

$$\overline{T}_{b,u} = S_u \frac{D'\,\lambda^2}{8\,\pi\,k} .$$

Since $2\,c = 1/\overline{T}_{b,u}$, we see that one unit on the polarization recorder is equal to a polarization full-beam brightness temperature of $\overline{T}_{b,u}^p = 2\,\overline{T}_{b,u}$.

To calibrate the receiver, the point sources Cas A, Cyg A and Tau A were measured with respect to nearby comparison fields several times each throughout the observing period, using the total-power recorder. The two detector laws were found equal to within a few per cent over the limited range over which they were used. Their average may be written as

$$c.W = E + 2.80 \times 10^{-4}\, E^2,$$

where W is the input power and E is the output voltage of the detector in our units. The gains of the two halves of the receiver were maintained equal. After correction for the detector law, the recorder deflection for Cas A was found to be 3735 ± 60 units with respect to its immediate surroundings. The deflection close to Cas A was 10600 units. Assuming Cas A to have a flux density of 5600×10^{-26} Watts m^{-2} $(c/s)^{-1}$ (SEEGER 1956), we find that a recorder deflection of 1 unit corresponds to $S_u = 1.50 \times 10^{-26}$ Watts m^{-2} $(c/s)^{-1}$.

To calculate the full-beam brightness temperature $\overline{T}_{b,u}$ giving a deflection of 1 unit we have to derive the value of the beam directivity D' from the antenna pattern. This was measured simultaneously but separately for both planes of polarization in the 8 positions of the feed, using the quiet sun as a source. In all cases, the first side lobes were found to be more than 27 db below the main lobe. A sample set of patterns is shown in Figure 11. To arrive at a value for D', a few of these antenna patterns were integrated within radii of 1, 2, 3, 5 and 10 degrees. The main beam is closely Gaussian down to 20 db. After corrections for broadening of the beam by the sun's finite extent (2 per cent in beamwidth) the beamwidths are $\theta_E = 2°.01$ and $\theta_H = 2°.09$. The beam solid angle, Ω', in square degrees, and the values of D' are given in Table 4 for circular areas with various radii around the centre of the beam. Outside the 10° radius, the near side lobes are practically all well below 40 db. For comparison the value of Ω' in square degrees for a Gaussian beam with the same halfwidths is also given. We shall define as the full beam the area for which $D' = 8500$. Using the value of S_u derived above, we then find that a deflection of 1 unit on the total-power recorder corresponds to an increase in full-beam brightness temperature of $\overline{T}_{b,u} = 0.20$ °K. A deflection of 1 unit on the polarization recorder corresponds to an increase in polarization full-beam brightness temperature of $\overline{T}^{p}_{b,u} = 0.40$ °K.

TABLE 4

Antenna pattern characteristics.

radius	$\Omega'_{Gaussian}$	$\Omega'_{real\ beam}$	D'
1°	2.30□	2.30□	17900
2	4.41	4.41	9350
3	4.75	4.75	8690
5	4.76	4.81	8570
10	4.76	4.89	8450

FIGURE 11

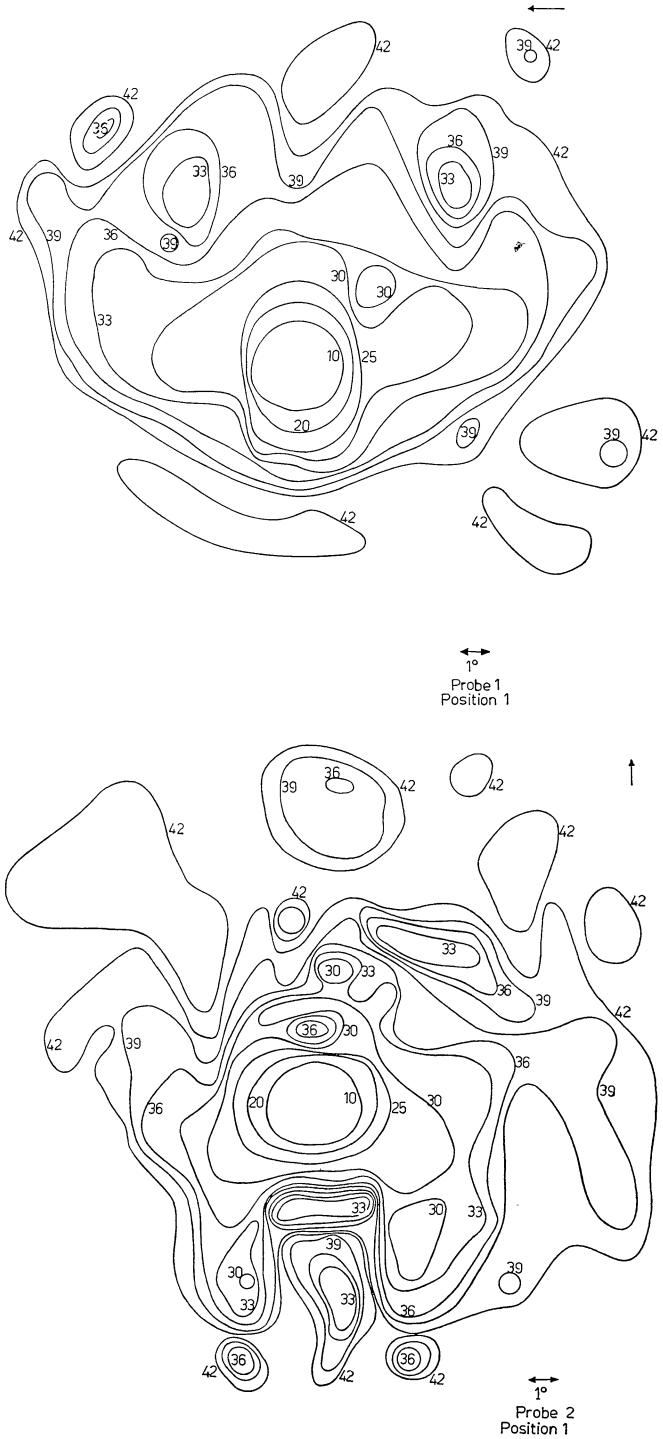

Antenna patterns for probe 1 and probe 2, using the sun as a source, in db below the main beam.

For an evaluation of the effects of radiation in the far sidelobes, it is useful to make an estimate of the stray factor $\beta = 1 - D/D'$, the fraction of the received power incident from directions outside the full beam. If the antenna temperature of Cas A could be measured accurately, D and thus β could be found from

$$T_A = \frac{\eta_R \lambda^2}{8\pi k} \cdot D \cdot S,$$

which follows from the definitions at the beginning of this chapter, with

$$S = \frac{2k}{\lambda^2} \int_{\text{source}} T_b \, d\Omega .$$

The value of T_A may be calculated from the relation

$$\frac{W_{(\text{receiver + background + Cas A})}}{W_{(\text{receiver + background})}} = \frac{[T_A(\text{Cas A}) + T_A(\text{background})]\,\alpha + (1-\alpha)\,T_0 + T_R}{[T_A(\text{background})]\,\alpha + (1-\alpha)\,T_0 + T_R},$$

where the left-hand term is found from the recorder deflections by correcting these for the detector law. The term T_A (background) contains contributions from the radiation underlying Cas A, and from radiation of the sky and the ground in the side lobes. From the contour map of the background radiation (Figure 10) we find that the radiation underlying Cas A has a brightness temperature of the order of 50 °K, and with $\beta = 0.15$ (see below), $T_A = 42$ °K. The ground and sky radiation in the side lobes is very difficult to estimate. We shall assume that it contributes about 30 °K to T_A, so that T_A (background) ≈ 75 °K. Unfortunately only a very rough determination of the receiver noise temperature T_R and the attenuation α between feed and receiver input was made. With a value of 1.61 for the ratio of total power on and off Cas A, a noise figure $N = 3.8$, giving $T_R = 840$ °K, an attenuation of 0.8 db (factor 0.83), and $T_0 = 280$ °K, we find T_A (Cas A) $= 698$ °K. Assuming $\eta_R = 0.98$ this leads to $D = 8090$ and $\beta = 0.05$.

Another way of finding β is by measuring the effect of ground radiation in the spillover lobes. A number of sweeps in elevation were made which, after correction for sky radiation, showed that after a sharp drop between elevation 0° and 20°, and a constant value between 20° and 50°, the intensity rose by about 10 °K between elevation 50° and 90°. The angle at which the feed sees the edge of the dish is 55°. If we assume that most of the back lobes are due to direct spillover around the edge of the dish, they must be mainly concentrated between $\theta = 90°$ and 125° and occupy a solid angle of about 10000 square degrees, i.e. 2000 times the size of the full beam. We estimate that at elevation 50° two thirds of this solid angle covers the ground, at high elevations all of it. Therefore, a solid angle of 700 times the full beam, looking at the ground which might have a brightness temperature of 250 °K, causes a rise in apparent brightness temperature of 10 °K between elevations 50° and 90°. The average sensitivity thus is $\frac{10}{250 \times 700} = 6 \times 10^{-5}$, so that the sidelobes occupy an equivalent solid angle of $\int f(\theta, \varphi)\, d\Omega = 6 \times 10^{-5} \times 10^4 = 0.6$ square degrees. The value of β so derived is $\beta = 1 - \frac{4.9}{4.9 + 0.6} = 0.11$. This is obviously a lower limit, since it only includes lobes which have $\theta > 90°$.

We arrive at a similar lower limit if we compare the apparent brightness temperature at elevation 0°, $T(h = 0°)$ with that at elevation 90°, $T(h = 90°)$. If we divide the lobe pattern into full beam, front lobes (between $\theta = 10°$ and 90°) and back lobes, then, not taking into account the radiation from the air,

$$T(h = 0°) \propto \tfrac{1}{2} \int_{\text{full beam}} f\,d\Omega + \tfrac{1}{2} \int_{\text{front lobes}} f\,d\Omega + \tfrac{1}{2} \int_{\text{back lobes}} f\,d\Omega ,$$

$$T(h = 20°) \propto \tfrac{1}{2} \int_{\text{front lobes}} f\,d\Omega + \tfrac{1}{2} \int_{\text{back lobes}} f\,d\Omega ,$$

$$T(h = 90°) \propto \int_{\text{back lobes}} f\,d\Omega .$$

From this,

$$T(h = 0°) - T(h = 20°) \propto \tfrac{1}{2} \int_{\text{full beam}} f\,d\Omega = \tfrac{1}{2}\Omega'$$

and

$$T(h = 90°) - T(h = 20°) \propto \tfrac{1}{2} \int_{\text{back lobes}} f\,d\Omega - \tfrac{1}{2} \int_{\text{front lobes}} f\,d\Omega = \tfrac{1}{2}(\Omega - \Omega') - \int_{\text{front lobes}} f\,d\Omega .$$

The ratio of these two measurable quantities is

$$\frac{\Omega'}{\Omega - \Omega' - 2\int_{\text{front lobes}} f\,d\Omega} .$$

If we assume that most of the radiation outside the full beam is due to the back lobes, then this ratio gives us a lower limit for Ω/Ω' and thus for $\beta = 1 - \Omega'/\Omega$. We find that $T(h = 0°) - T(h = 20°) \approx 120$ °K and $T(h = 90°) - T(h = 20°) \approx 10$ °K, which leads to $\beta > 0.08$. The value of β will increase due to the effect of the radiation from the atmosphere close to the horizon which increases the term $T(h = 0°)$ because the half of the full beam above the horizon is partially filled, and due to the non-zero value of the front lobes.

Theoretical calculations and measurements of the

radiation pattern of the feed show that the fraction of its radiation which misses the paraboloid is about 0.10. If there are no other causes of stray radiation, then $\beta = 0.10$. This is again a minimum value.

It is clear that the value $\beta = 0.05$ derived from the very uncertain measurement of the antenna temperature of Cas A is too low. The values $\beta > 0.11$ and $\beta > 0.08$ derived from the ground radiation effects are lower limits, as is the value $\beta = 0.10$ derived from the primary pattern of the feed. It is impossible to derive an upper limit for β, but it seems safe to assume that β is of the order of 0.15. In that case, $\eta_B = \eta_R(1-\beta) = 0.83$ with $\eta_R = 0.98$, and the antenna efficiency $\eta_A = \eta_B \frac{\lambda^2}{A_g \Omega'} = 0.61$, a reasonable value. If $f(\theta, \varphi)$ is constant outside the full beam and $\beta = 0.15$, we have $f(\theta, \varphi) = 2 \times 10^{-5}$. In the case of a concentration of sidelobes within $\theta = 90°$ to 125°, the average value of $f(\theta, \varphi)$ in that area was found to be 6×10^{-5}. Sweeps through the sky during the daytime showed no solar radiation in small sidelobes outside the full beam, which puts an upper limit on $f(\theta, \varphi)$ of about 4×10^{-5}, confirming the estimates made above. We shall use $\beta = 0.15$ throughout this article.

5. *Spurious polarization produced by the imperfect antenna pattern*

The ideal antenna for measuring linear polarization in the typical radio-astronomical situation of interest here, has the following properties:

a) It is 100% linearly polarized in all directions.

b) The planes of polarization in all directions where the power response is non-zero intersect along a single line.

c) The power response, $f(\theta, \varphi)$, is circularly symmetric about the axis direction where $\theta = 0$ and $f(0,0) = 1$.

When such an antenna is rotated about its axis, no brightness distribution in the field of view can cause the observation of spurious polarization. Such an ideal antenna pattern cannot be produced. One cannot even produce an antenna with an orthogonally bi-symmetric pattern centred on $f(0,0) = 1$. Furthermore, because of constructional errors and analytical limitations, predicted performance can hardly be relied on. For measurements of the type considered here, only detailed pattern studies over all significant directions can suffice.

In this section we describe those pattern tests we performed in order to try and estimate the reliability of our polarization measurements. They were far from complete, in particular as the regions far from the axis are concerned. For those regions only estimates were made.

FIGURE 12

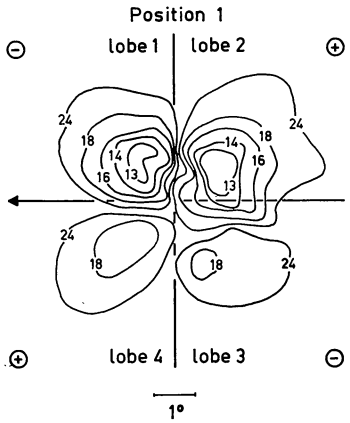

Antenna pattern, measured with the polarization channel, for unpolarized radiation, using Cas A as a source, in db below the main beam response for a single probe.

a) Full-beam sidelobes.

With the polarization receiver, sweeps were made through and around Cas A, showing the spurious polarization response occurring when a bright unpolarized source is situated in the vicinity of the main beam.

The resulting patterns, one of which is shown in Figure 12, were made for all positions of the feed. They show the same general pattern of four 45°-sidelobes. The cylindrical waveguide feed used here has as its main advantage that the cross-polarization side lobes in the ideal case are zero. That this pattern still resembles the cross-polarization pattern of a dipole feed is probably due to the position of the probes in the waveguide, rather close to its open end. For an ideal dish and a dipole feed the four cross-polarization lobes should be exactly equal. It was found that:

1) They differ in intensity by more than a factor of four.

2) There is an obvious difference between the lobes above and below the main beam, which may be due to sagging of the dish and bending of the mast, and the asymmetric position of the guy wires.

3) The lobe structures in two orientations of the feed separated by 90° and 180°, respectively, are not exactly equal, showing that despite our efforts to obtain rotational symmetry, the combination of feed, supporting mast and guy wires was not as symmetric as desired. From the antenna patterns measured with the two receivers separately (Figure 11) the same general conclusions could be reached.

In Figure 12 the quantity displayed is $F(\theta, \varphi)$, defined as the polarization antenna temperature relative

to the unpolarized antenna temperature when Cas A is at the centre of the main beam,

$$F(\theta,\varphi) = T_A^p(\theta,\varphi)/T_A(0,0)\ \text{(Cas A)} = \\ = \overline{T}_b^p(\theta,\varphi)/\overline{T}_b(0,0)\ \text{(Cas A)} = \\ = I_0(\theta,\varphi)/\tfrac{1}{2}I_T(0,0)\ \text{(Cas A)}.$$

Table 5 lists the maximum values of $F(\theta, \varphi)$ for each lobe separately in the eight feed positions. The lobes are numbered 1 to 4 as in Figure 12, and rotate anticlockwise between positions 1 and 8. If a point source is situated in the maximum of lobe 1 in position 1, rotation of the feed will cause lobe 2 to be on the source in position 3, lobe 3 in position 5 and lobe 4 in position 7. The measured values of $F(\theta, \varphi)$ are of the same order of magnitude as those calculated for a dipole feed in the Dwingeloo telescope.

TABLE 5

Maximum value of $F(\theta, \varphi)$ for the four 45°-sidelobes.

Feed position	lobe 1	lobe 2	lobe 3	lobe 4
1	-5.8×10^{-2}	$+6.1\times10^{-2}$	-1.7×10^{-2}	$+2.4\times10^{-2}$
2	−4.7	+2.5	−3.6	+5.7
3	−3.2	+5.6	−6.4	+2.1
4	−6.9	+6.1	−1.5	+3.3
5	−1.6	+3.0	−6.4	+6.9
6	−3.5	+7.1	−7.2	+1.6
7	−6.7	+3.6	−3.1	+5.6
8	−2.5	+3.8	−6.7	+5.0

The data in Table 5 show that point sources causing a full-beam brightness temperature < 15 °K and thus having a flux density < 0.02 times that of Cas A would have caused a spurious polarization < 1 °K and would therefore have gone unnoticed. We checked whether any of our measured points was near a point source above 5 °K; this was so in three cases, which are noted in Table 3. If pointed at an extended region of brightness temperature T_b, each lobe would cause a spurious polarized signal of

$$\overline{T}_b^p = \int_{\text{lobe}} T_b F(\theta,\varphi)\, d\Omega/\Omega'.$$

Since all lobes have the same halfwidth of 1°.6 to within 10%, and a shape which is roughly Gaussian, we may write

$$\int_{\text{lobe}} F(\theta,\varphi)\, d\Omega = F(\theta,\varphi)_{\max}\cdot\Omega_{\text{lobe}},$$

where $\Omega_{\text{lobe}} = 2.9$ square degrees. With $\Omega' = 4.9$ square degrees, we find for a constant background temperature of 50 °K underlying all lobes a spurious polarization with $\overline{T}_b^p$ of the order of 0.7 °K (1.7 units). If the background temperature increases from 100 °K to 150 °K over two degrees, as might be the case in some regions near the Milky Way, spurious signals of the order of 2.5 °K (= 6 units) are to be expected. The conclusion that the effects of the near-in sidelobes may be neglected is strengthened by the observation that a few runs across the Milky Way showed no large values, nor large variations of the polarized signal.

b) Far sidelobes on the sky.

If the whole sky (i.e. half the sphere) has a constant brightness temperature T_b, and the value of $f(\theta, \varphi)$ is constant, on the average, in all directions outside the full beam, the contribution of the sidelobes outside the full beam to the antenna temperature is $T_A = \eta_R \frac{\beta}{2} T_b$. We assume $\beta = 0.15$. Then, if a region such as the central part of the Milky Way, with an area of say $100 \times 10 = 1000$ square degrees (i.e. 0.05 of the hemisphere) and a brightness temperature of 150 °K, rises above the horizon, the antenna temperature increases by an amount $\Delta T_A = \eta_R \frac{\beta}{2} T_b \times 0.05 = 0.55$ °K. In the unlikely case that all sidelobes looking at the Milky Way are cross-polarization lobes with one polarity, this temperature rise is observed as a spurious polarized signal.

It was shown in Chapter 4 that if all sidelobes are concentrated in a ring between $\theta = 90°$ and 125°, the value of β deduced from the ground radiation effect is 0.11. If the region of the Milky Way assumed above falls entirely within this ring, it occupies 0.1 of its solid angle. Again, if all of this solid angle is polarized, this causes a rise in antenna temperature of $\Delta T_A = \eta_R \beta\, T_b \times 0.1 = 1.6$ °K.

c) Far sidelobes on the ground.

If the value of $f(\theta, \varphi)$ is constant outside the full beam, and $\beta = 0.15$, the antenna temperature caused by the radiation from the ground, assuming it to be a black body with temperature $T_0 = 280$ °K, is $T_A = \eta_R \frac{\beta}{2} T_0 = 21$ °K. If all sidelobes are concentrated between $\theta = 90°$ and 125°, we have, if the telescope is pointed at the zenith, $T_A = 30$ °K, and if the telescope is pointed at the horizon, $T_A = 15$ °K. On the basis of the present measurements and tests it is completely impossible to judge in how far this radiation is linearly polarized, or whether the relevant sidelobes are polarized. In Chapter 3 (Figure 8) we showed that we observe elevation-dependent spurious polarization with an apparent $\overline{T}_b^p$ varying between 0 and 4 °K, which therefore may be attributed to radiation from the ground in the far sidelobes.

6. *Synchrotron radiation from the VAN ALLEN belts and the interplanetary medium*

The radiation from the VAN ALLEN belts and the interplanetary medium is shown in the following to be negligible. To calculate the emission from the VAN ALLEN belts we make the following assumptions:

a) We measure at a point on the earth's equator.

b) The magnetic field runs in the same direction everywhere, in a plane parallel to the surface of the earth.

c) The velocity distribution of the electrons is isotropic.

d) The energy spectrum of the electrons is of the form: $n(E)\,dE = AE^{-\beta}\,dE$.

e) The earth's magnetic field can be represented by $H = H_0 R^{-3}$, where R is the distance from the centre of the earth.

f) The antenna pattern has a rectangular cross-section, with a width α radians ($f(\theta, \varphi) = 1$ for $\theta \leq \frac{1}{2}\alpha$, $f(\theta, \varphi) = 0$ for $\theta > \frac{1}{2}\alpha$).

If the energy radiated per electron per second per c/s is $P(\nu)$, then the energy received in the antenna beam is, per cm² of antenna:

$$W(\nu) = \int_{R=R_0}^{\infty} \int_{E=E_1}^{E_2} \frac{\alpha^2}{16} P(\nu)\, n(E)\, dE\, dR \text{ erg (c/s)}^{-1}\text{sec}^{-1}\text{cm}^{-2},$$

where R_0 is the earth's radius and E_1, E_2 are the lower and upper limits of the energy distribution. If we assume $E_1 = 0$ and $E_2 = \infty$, then, according to SHKLOVSKI (1960),

$$\int_{E=0}^{\infty} P(\nu)\, n(E)\, dE = \frac{12\, e^3 H}{mc^2} \left(\frac{eH}{\pi m^3 c^5}\right)^{\frac{\beta-1}{2}} \nu^{\frac{1-\beta}{2}} A\, u(\beta),$$

where $u(\beta)$ is a function of β tabulated by SHKLOVSKI. For $\nu = 408$ Mc/s:

$$\int_{E=0}^{\infty} P(408)\, n(E)\, dE =$$

$$1.63 \times 10^{-21} (2.0 \times 10^{10})^{\frac{\beta-1}{2}} H^{\frac{\beta+1}{2}} A\, u(\beta),$$

hence

$$W(408) =$$

$$\int_{R=R_0}^{\infty} 1.63 \times 10^{-21} \frac{\alpha^2}{16} A\, (2.0 \times 10^{10})^{\frac{\beta-1}{2}} H^{\frac{\beta+1}{2}}\, u(\beta)\, dR.$$

According to SONETT *et al.* (1960) we can represent the earth's magnetic field by $H = 9.0 \times 10^{25}\, R^{-3}$ oersted up to at least 9 earth radii. From the data given by VAN ALLEN *et al.* (1959) we calculate for the inner belt: $\beta = 3$, $A = 4 \times 10^{-15}$; for the outer belt: $\beta = 4$, $A = 10^{-21}$. We assume: for each belt the density distribution in the line of sight is rectangular; the thickness of the inner belt is 9.6×10^8 cm and of the outer belt 1.6×10^9 cm; the width of the antenna pattern $\alpha = 0.03$ radians. Then,

$$W(408) = 5 \times 10^{-24} \text{ erg (c/s)}^{-1}\text{sec}^{-1}\text{cm}^{-2}$$
$$= 5 \times 10^{-27} \text{ watts m}^{-2}\text{ (c/s)}^{-1}.$$

Using the data given in Chapter 4, we find that this corresponds to a brightness temperature of 0.1 °K.

However, there seems to be an indication that at higher energies the energy spectrum of the electrons is steeper than at lower energies. The number of electrons with energies around 50 MeV, which are mainly responsible for synchrotron radiation at 408 Mc/s, is thus smaller than would be expected from observations at low energies. Hence the flux density is lower than calculated above (see for instance VERNOV *et al.* 1959, who find $\beta = 6$, which yields $T_b = 0.5 \times 10^{-6}$ °K). Furthermore, electrons can only be trapped in the upper VAN ALLEN belt if they have an energy less than 700 MeV (STÖRMER cut-off), and hence the number of electrons with energies of about 50 MeV is already smaller than would be expected from an ideal exponential energy distribution.

At lower frequencies it is possible that the VAN ALLEN belts may have some influence on the observed polarization, especially during periods of high solar activity.

If we assume that the energy spectrum of the electrons and the magnetic field are constant throughout the solar system, and that the magnetic field is randomly oriented, then, according to SHKLOVSKI (1960), the brightness temperature due to emission from a path length L (cm) is:

$$T_b = \frac{3\, e^3}{2\pi k \nu^2 m} \left(\frac{e}{\pi m^3 c^5}\right)^{\frac{\beta-1}{2}} \nu^{\frac{1-\beta}{2}} H^{\frac{\beta+1}{2}} A\, u(\beta)\, L.$$

For $\nu = 408$ Mc/s and $H = 3 \times 10^{-4}$ oersted (VAN ALLEN 1959, VERNOV *et al.* 1959) we find:

$$T_b = 0.78 \times 10^{-6}\, (8.3 \times 10^6)^{\frac{\beta-1}{2}} A\, L\, u(\beta).$$

In the outer VAN ALLEN belt the flux of electrons with $E > 20$ keV is 10^{11} cm^{-2} sec^{-1}. Assuming that the flux of these electrons in the interplanetary medium is 10^7 cm^{-2} sec^{-1}, we can calculate A and T_b for different values of β. Taking the orbit of Pluto ($L = 6.4 \times 10^{14}$ cm) as the outer limit of the interplanetary medium, we find values for T_b ranging from 4×10^{-2} °K for $\beta = 2$ to 2×10^{-15} °K for $\beta = 6$.

Although these values are rather sensitive to the assumed values of the density of relativistic electrons and of β, it is clear that the observed polarization cannot be due to the VAN ALLEN belts or the interplanetary medium.

7. *Faraday rotation in the ionosphere*

Faraday rotation is the rotation of the plane of polarization caused by the presence, at the same place, of an ionized medium and a magnetic field with a component along the direction of propagation. It results from the difference between the optical path lengths traversed by the ordinary and extraordinary waves. Assuming we may use the quasi-longitudinal approximation of the magneto-ionic theory, we derive the sense and magnitude of the rotation as follows:
Let the ordinary wave vector rotate clockwise, the extraordinary anti-clockwise, and let the wave incident on the magneto-ionic medium be polarized along *AA* (Figure 13). Then α_o and α_x denote the ordinary and extraordinary incident field vectors at some given time *t*. On emerging from the medium, the vectors will be in new positions. Let β_x be the extraordinary wave vector. Since the refractive indices are related by $n_o > n_x$ (see for example BROWNE *et al.* 1956), the ordinary wave takes longer to traverse the medium than the extraordinary. Hence β_x does not combine with β_o, the vector corresponding to the incident vector α_o, but with β_o', which corresponds to the incident vector at some earlier time than *t*. The resultant plane of polarization is *BB*, inclined to *AA* at an angle ξ equal to half the phase difference between the ordinary and extraordinary components, i.e. $\frac{1}{2} \cdot \frac{2\pi}{\lambda} \cdot L(n_o - n_x)$, where *L* is the physical path length within the medium. The sense of rotation is the same as that of the extraordinary wave.

In general appreciable Faraday rotation will take place both in interstellar space and in the earth's ionosphere. The interstellar rotation will be constant in time and cannot be determined by measurements at one frequency only. The ionospheric rotation, however, does vary, and this variation can be used to detect it. It is important to be able to do this, since it would provide proof that we are indeed observing polarized radiation from outside the earth's atmosphere, and not some spurious effect due to unpolarized radiation; a proof which is independent of any calculations or estimates of the antenna pattern. In our case, looking towards the source of the radiation, the components rotate in the sense shown in Figure 13 (MITRA 1948, p. 161 in first edition; BREMMER 1949, p. 324) for all except a small part of the sky (in the North, at elevations less than 30°). In general, therefore, the observed values of the polarization angle are larger than the values outside the ionosphere.

FIGURE 13

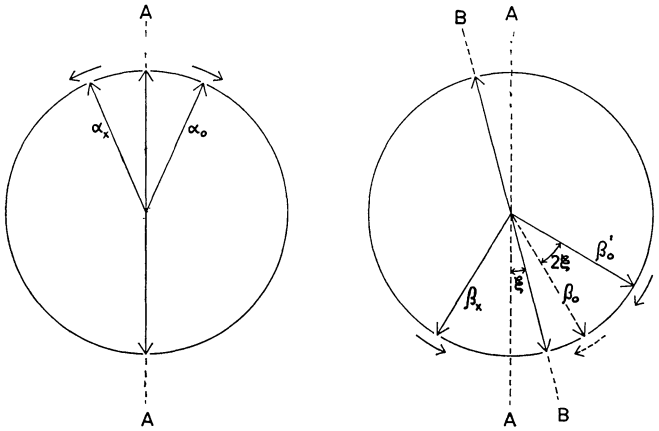

Schematic representation of Faraday rotation; see text.

Neglecting the curvature of the ionosphere, and using the quasi-longitudinal approximation, which is good enough for our present purpose, we have (BROWNE *et al.* 1956)

$$\xi = \frac{e^3}{2\pi m^2 f^2 c^2} \int_{\text{ray path}} N \,.\, H \cos \Phi \,.\, \sec z \,.\, dh \,,$$

where ξ = Faraday rotation (radians)
z = zenith distance of source
Φ = angle between magnetic field and direction of propagation
H = magnetic field (oersted)
N = number of electrons per cm^3
h = height above the earth (cm)
f = frequency of the radiation (c/s)
e = charge of the electron (ESU)
c = velocity of light (cm/sec)
m = mass of the electron (g)

Both z and Φ vary along the ray path, but since in general N is not accurately known, we may take for z and Φ their ground-level values z_o and Φ_o without affecting the total accuracy appreciably. Similarly, a mean value of H for the ionosphere is sufficiently accurate. The value chosen is for a height of 300 km, approximately at the maximum of the F_2 layer. We have

$$\xi = \frac{e^3}{2\pi m^2 f^2 c^2} H_{300} \cos \Phi_o \sec z_o \int N \, dh$$

and

$$\sec z_o \cos \Phi_o = \sin i + \cos i \tan z_o \cos (a + \beta),$$

where i = angle of dip of the magnetic field
β = magnetic declination (West)
a = azimuth of the source.

For Dwingeloo, for 1960 (VELDKAMP 1951),

$i = 68°$
$\beta = 5°$
$H_{300} = 0.41$ oersted (assuming the field falls off as the inverse cube of the distance to the centre of the earth).

Data on the value of $\int N \, dh$ can be obtained from two sources:

a) Moon radar echoes obtained at Jodrell Bank indicate a value of 5×10^{12} electrons per cm^2 at the pre-sunrise minimum and 50×10^{12} electrons per cm^2 in the first hour or so after sunset (EVANS and TAYLOR 1961). On this basis we should expect a Faraday rotation of between $\{0.27 + 0.11 \tan z_0 \cos (a + 5°)\}$ radians, and ten times that value. For the North pole these limits are 10° and 100°. The observed total range of variation of the polarization angle at the North pole is 70°; inaccuracies in the measurements and reduction are estimated to account for 30°.

b) Vertical ionosonde records taken at the Dutch Meteorological Institute, K.N.M.I., De Bilt, can be used to estimate $\int N\,dh$ at all times. If a parabolic distribution of electron density with height is assumed, then:

$$\int_{200\text{ km}}^{1000\text{ km}} N\,dh = 16.5 \times 10^{-9} (f_0F_2)^2\, y_mF_2 \text{ electrons per cm}^2,$$

where f_0F_2 = ordinary wave critical frequency of the F_2 layer (c/s)

and y_mF_2 = half-thickness of parabola at zero electron density (cm).

It is known that the F_2 layer profile is not parabolic; the value of $\int N\,dh$ calculated in this way is about one half of that actually observed (EVANS 1956). However, if this proportionality factor is more or less constant, the ionosonde data can be used to detect the effect of Faraday rotation in our measurements. Figure 14 shows the observed polarization angle (of which the value in the absence of rotation is unknown) plotted against the Faraday rotation to be expected from a parabolic layer having the observed critical frequency and half-thickness. Since values of the half-thickness are not available for all hours on all days, and individual measurements are not very reliable in any case, median values for each hour, calculated for the period November 26 to December 23, 1960, were used, interpolated between hours where necessary. This probably causes a maximum error of 40% in the values of the calculated rotation. The maximum error in the observed values of the polarization angle, due to errors inherent in the measurements and reductions, is about 15°. (Note that the mean errors quoted in Chapter 3 include the effects of variation of Faraday rotation with time.)

The North pole points were obtained from nights on which the instrumental effects remained constant and thus the ends of all the North pole vectors fell on a circle with the previously derived standard radius, chosen without reference to the angular displacement of the points on the circle. Using the centre of the circle as instrumental zero error, the polarization angles were measured and corrected for the rotation of the sky relative to the telescope to give the values

FIGURE 14

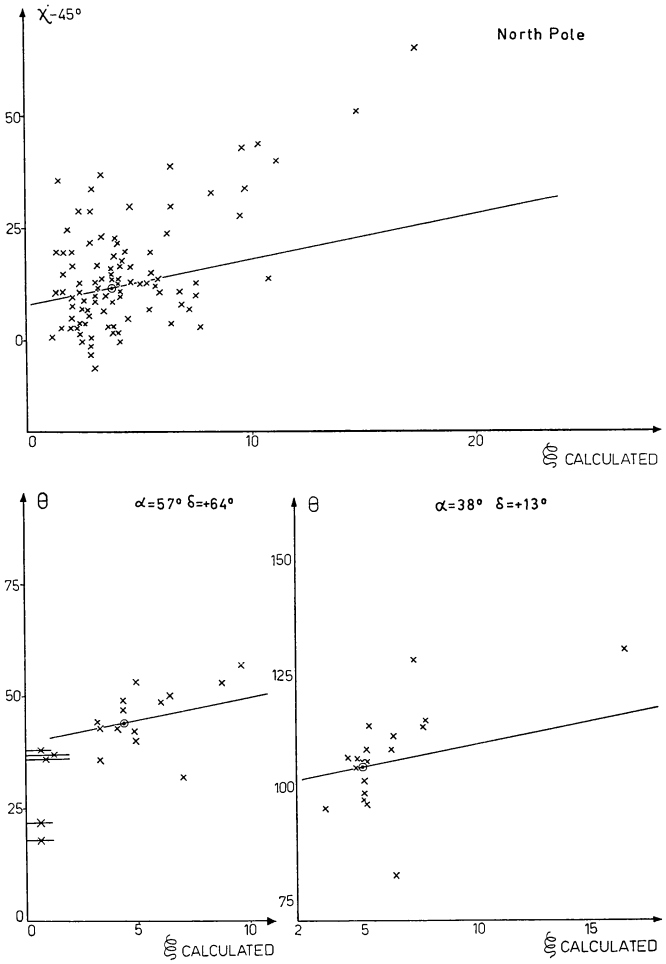

Observed polarization angle and ionospheric Faraday rotation expected for a parabolic F_2 layer. The points would coincide with the straight lines of unity slope if the F_2 layer were in fact parabolic.

plotted in Figure 14. For the two other points the measurements were reduced in the normal way. The straight lines have a slope of unity and go through the centre of gravity of the cluster of points at low values of rotation. They would be expected to represent all the points if the F_2 layer were parabolic. Any departures will show up most strongly at high values of rotation, far away from the artificial agreement at the lower values.

From each of the graphs separately, we conclude that:

a) There exists a systematic change of polarization angle with expected value of Faraday rotation. This change is in the direction predicted by theory.

b) The slope of any line representing the points lies between 1.5 and 5, and if we are to explain this as due to Faraday rotation, the ratio of total electron content to electron content of a parabolic layer must lie between these same limits.

Although the high values of rotation systematically occur early in the night, and the temperature (to which the equipment is expected to be sensitive) is generally higher early in the night, it is unlikely that any instrumental effect could have caused the observed variations. In this case both angle and intensity variations would be expected, whereas only systematic angle variations are apparent.

In principle, the value of the polarization angle outside the earth's atmosphere may be found from plots like Figure 14. Only in the case of the North pole has this been done.

8. *The polarization of the continuous background radiation*

In this section we shall discuss the results of our observations, which are given in Table 3 and Figure 10, with the exception of those of the discrete sources. With the aid of Tables 1 and 2 the reliability of the data may be assessed. Figure 10 shows that only a very limited part of the sky was investigated. The main survey consists of observations at declinations $+12°.5$ and $+64°$, and occasional observations at neighbouring declinations. Only in a small region around $l^{II} = 140°$, $b^{II} = +5°$ is the coverage complete, i.e. the observed points are spaced closer than the beamwidth of 2°. The observations in which we have some confidence and which in general have intensities ≥ 5 units, are plotted as small lines; at all other positions where observations were made, a dot is plotted.

The regions in which measurements were made were in general selected because either the intensity there was high or because the region was of particular interest for some other reason. Any conclusions based on such incomplete and subjectively selected material might be considered doubtful. We feel, however, that the material allows a general discussion and some conclusions, in particular since such a discussion might indicate requirements for future observations.

The plane of polarization suffers Faraday rotation when the radiation passes through regions where matter is ionized and a magnetic field is present. From the formula given in Chapter 7, we find for the total number of rotations n of the plane of polarization over 360° at a frequency of f Mc/s:

$$n = 0.73 \times 10^5 \times N \times H_{\parallel} \times L \times \left(\frac{408}{f}\right)^2,$$

where L is the path length in parsecs, N is the electron density in cm^{-3} and $H_{\parallel}$ is the component of the magnetic field in the line of sight, in oersted.

The mean density of ionized gas in the Galaxy is not well known. From a study of the thermal component of the continuous radio emission from the galactic plane, WESTERHOUT (1958) derived smoothed values of the emission measure $E = \int N^2 dL$, per kpc, as a function of R, the distance to the galactic centre. Near $R = 8$ kpc, he finds an average value $N^2 = 0.15$ cm^{-6}. If the ionized gas is smoothly distributed, this leads to $N = 0.4$ cm^{-3}. In the more probable case of concentration of ionized matter into clouds, the total average space density might be anywhere between 0.1 and 0.01 cm^{-3} or even lower.

The observation that the position angle of the plane of polarization of the Crab Nebula, Tau A, does not change by more than 20° between wavelengths of 3 and 10 cm (MAYER *et al.* 1957, 1960), gives an upper limit for the value of $\overline{NH}_{\parallel}$ between the sun and this nebula. Assuming a distance of 2000 pc, and taking into account the fact that Tau A is situated about 200 pc below the galactic plane, we may take for the length of the path through the gas layer in the disk $L = 1000$ pc. If the total rotation of the plane of polarization at 10 cm is 25°, it follows that $\overline{NH}_{\parallel} = 5 \times 10^{-8}$, from which $\overline{N} = 5 \times 10^{-3}$ cm^{-3} for $H_{\parallel} = 10^{-5}$ oersted and $\overline{N} = 5 \times 10^{-2}$ cm^{-3} for $H_{\parallel} = 10^{-6}$ oersted.

If the radiation traverses a medium with a density of this order, say $N = 10^{-2}$ cm^{-3}, and a field of $H = 10^{-5}$ oersted, then a path length of 100 pc causes the polarization vector at 408 Mc/s to rotate over $0.73 \times 360°$. An interstellar cloud with $N = 1$, a diameter of 10 pc and $H = 10^{-5}$ gives 7.3 full rotations and because of the normal irregularities in the density will depolarize the radiation entering the 2° beam of the radio telescope completely. Therefore, the radiation *must* originate between the observer and the nearest ionized cloud.

It is generally assumed that a line of sight in the galactic plane meets a few ionized clouds per kiloparsec. Observed average clouds of ionized gas have densities of the order of 1 to 10 ions per cm^3. It seems reasonable to assume the existence of clouds with even smaller densities, perhaps rather extended. A cloud with $N = 1$ and a diameter of 50 or 100 pc would be practically unobservable optically. The cloud complex in the Vela-Puppis region is a good example of an extended ionized region. All radiation from behind such a cloud is completely depolarized and clouds like that in Vela-Puppis, or even considerably less dense, form an effective screen against which we might observe polarized radiation. It seems reasonable to assume that such a screen exists at varying distances up to a few hundred parsecs, at least in all directions in the galactic plane.

It may be shown that the radiation originating in such a small volume around the sun may still be a considerable fraction of the total continuum radiation received from the galactic plane and the halo. For, if the sun is situated inside a spiral arm, and if the non-

thermal radiation from the galactic disk is mainly concentrated in the arms, the radiation from the local arm may reach intensities up to 20 or 30 per cent of the total nonthermal radiation in some directions.

It is therefore not surprising that we observe degrees of polarization up to 10 per cent in particular regions. It may be that in those directions the density of ionized gas near the sun is smaller than in most other directions, so that the depolarization due to interstellar Faraday rotation is less severe.

It is interesting to compare our results with observations of the polarization of star light. In Figure 15 we have plotted some of the data on optical polarization given by HALL (1958). In some instances there seems to be an indication that his vectors, which give the direction of the electric vector, i.e. that of the magnetic field if the DAVIS-GREENSTEIN mechanism holds, tend to be perpendicular to ours. This shows that in those regions there might be detailed agreement between the direction of the magnetic field derived from optical and radio polarization, and the interstellar Faraday rotation must be very small. Most of the stars measured in the optical work are within 500 parsec from the sun, and the polarization of their light must be connected with the same magnetic fields that cause the synchrotron radiation.

Unfortunately, not enough measurements have been made yet to permit detailed study of the relation between the magnitude and direction of the polarized component and the intensity of the unpolarized background radiation. The main conclusion one can draw from a study of the maps in Figure 10 is that there is not much, if any, correlation between these quantities. This again suggests that the region in which the polarized component originates is small compared with the Galaxy.

The series of measurements at and around declination + 12°.5 was made to cover the feature of galactic radiation which emerges at right angles from the Milky Way at $l^{II} = 32°$ ($l^{I} = 0°$). It may be seen that the intensity of the polarized component at the position of this "spur" is not significantly different from the intensity at other points in the sky. Because the "spur" and its surroundings were not fully covered with measurements we cannot definitely establish that there is no correlation between polarized and unpolarized components. It is, however, certainly not an outstanding phenomenon on the polarization map. It might therefore well be that the "spur" is not close to the sun and possibly outside the local region discussed before, i.e. at a distance greater than 50 to a few hundred parsec.

In the planning of future observations, the following points should be especially emphasized:

FIGURE 15

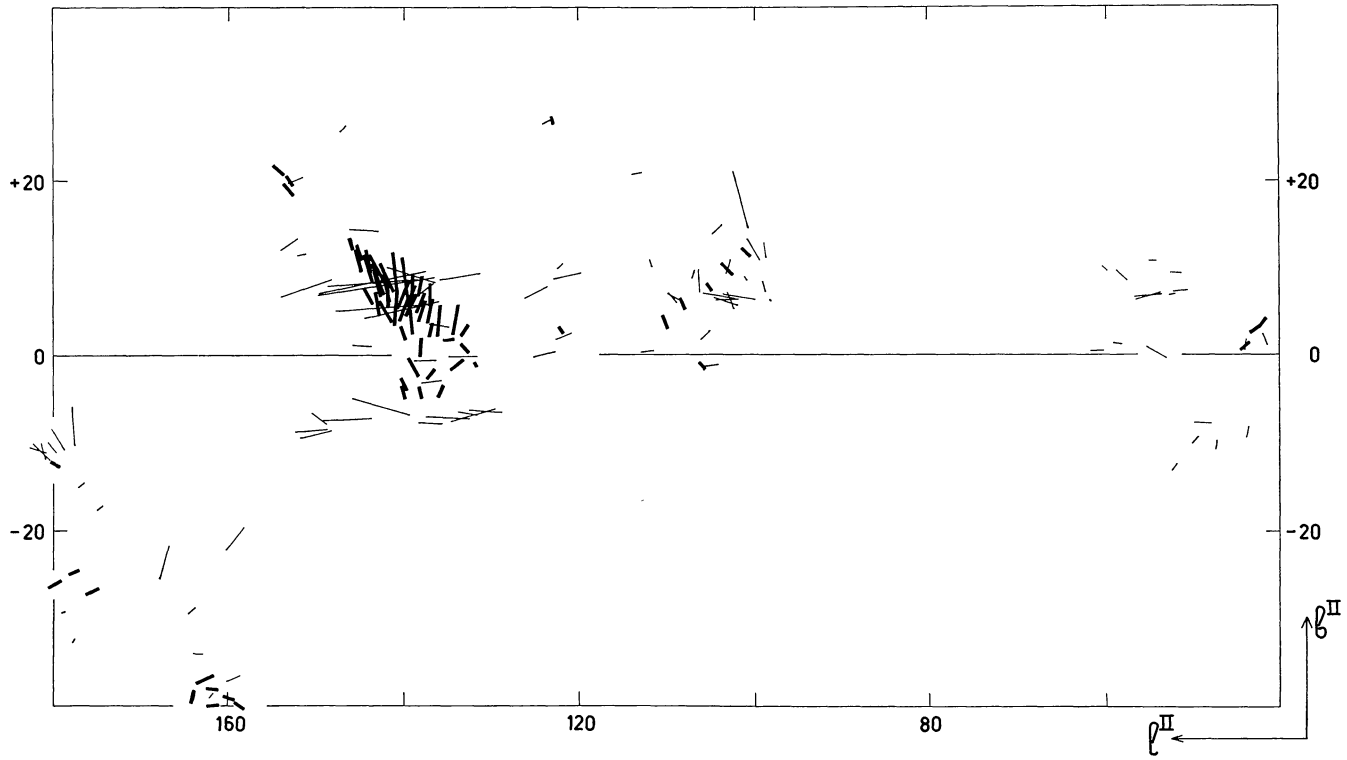

Comparison of radio (thick lines) and optical (thin lines) polarization (HALL 1958). The position angle of the lines is that of the electric vector. The DAVIS-GREENSTEIN mechanism predicts optical electric vectors parallel to the magnetic field. Radio electric vectors are perpendicular to the field.

1) The ionospheric Faraday rotation will have to be determined as accurately as possible. One of the ways in which this can be done, namely by measuring points with a high polarization temperature at times when the rotation changes rapidly, is indicated in Chapter 7.

2) Effects of ground and sky radiation in far sidelobes should be minimized, and a major effort should go into their determination.

3) Interstellar Faraday rotation may be determined by observing at different frequencies, provided the ionospheric Faraday rotation can be determined accurately. If the Faraday rotation at 408 Mc/s is as small as the correlation between radio and optical polarization angles in some places suggests, the shift in frequency may have to be considerable, i.e., of the order of tens of megacycles per second. Measurement of the interstellar Faraday rotation will give the polarity of the magnetic field, and an estimate of the product $\overline{NH}$.

4) Measurements should extend over the whole visible sky to obtain information about the structure of the local magnetic field, the connection between polarized radiation and features in the unpolarized background, and the connection with optical polarization data.

5) By going to much higher frequencies one eventually increases the region around the sun in which the polarized radiation originates. It is to be expected that the first increase of the length of the line of sight and thus of the degree of polarization occurs within a small frequency range, when the nearest ionized cloud stops acting as a depolarizing screen. On the basis of the distribution and the assumed density and dimensions of the ionized clouds and the value of the magnetic field strength, we would expect this to occur at a different frequency in each direction but usually well above 1000 Mc/s, where unfortunately the intensity of the nonthermal radiation is very small.

9. *Point sources*

Measurements were made of the polarization at the position of the point sources Cas A, Tau A and Vir A. Due to the high intensity of these sources, even a slight misalignment of the telescope could cause appreciable deflections through radiation in the 45° sidelobes (see Chapter 5). Figure 16 shows the observations. For Tau A and Vir A the scatter is no larger than for other points in the sky. Cas A shows a scatter of 15 units in I_0 and 50° in θ. We estimate that these variations could be caused by misalignments of up to 0°.08 either way, a reasonable value to expect. The effect of similar misalignments on the weaker sources would be indistinguishable from the normal scatter. In addition, the Cas A points show a mean polarized intensity which would need a systematic misalignment of 0°.15 to explain it in the same way. Such a large misalignment seems highly improbable. The intensity of the polarized radiation at the position of Cas A is of the same order as that found in other parts of the sky. Observations with a single pencil beam antenna give the vector sum of the polarized radiation of the discrete source and of the background. These two cannot be separated, but the large signal at the position of Cas A is more likely to be due to the polarization of the surrounding background.

FIGURE 16

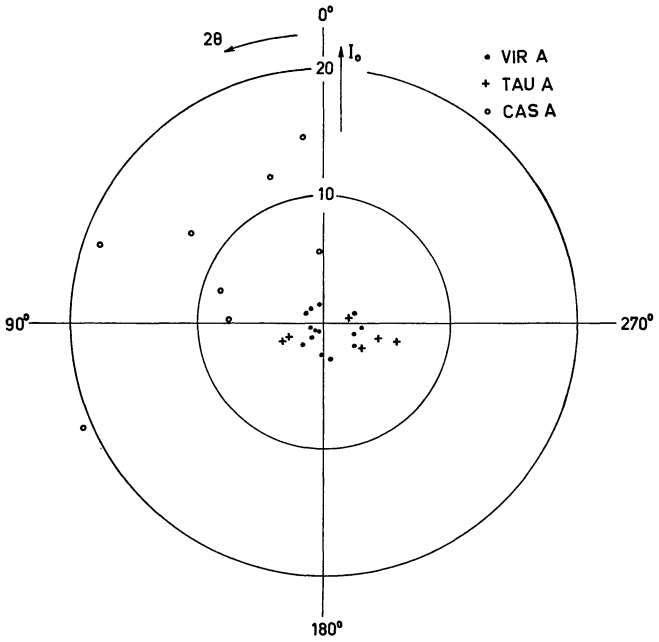

Individual observations of three point sources.

The centre of gravity of each set of points in Figure 16 is tabulated in Table 6. Also given are the full-beam brightness temperatures, $\overline{T}_b$, of the sources and of the surrounding background. The value of the upper limit of the degree of polarization at the position of the source is clearly a combination of the upper limits for the source and for the background.

Because of depolarization in the source we expect a much lower degree of polarization at our wavelength than has been found, for example for Tau A, at much shorter wavelengths.

TABLE 6

Polarization at the position of discrete sources.

Source	I_0 (units)	θ	$\overline{T}_b^p$ (°K)	$\overline{T}_b$ (°K)	$\overline{T}_b$ (°K)	degree of polarization
	at position of source			source	background	
Cas A	9.5±2.6	27°	3.8	747	50	< 0.4 %
Tau A	1.9±1.2	118	0.8	150	40	< 0.3
Vir A	0.6±0.4	110	0.2	60	24	< 0.2

10. *Comparison with other measurements*

There have been several reports of attempts to measure the polarization of the galactic background radiation. The equipment was different from ours in all cases, either in beamwidth, or in bandwidth, or in centre frequency, or any combination of these. The bandwidth is usually small enough to neglect its depolarizing effect on radiation which has suffered Faraday rotation (RAZIN (1958) used a wide band to obtain a zero level, but his actual measurements were made with small bandwidth).

Measurements made at the same frequency, but with different beamwidths, may be compared directly. We integrate the Stokes parameters for linearly polarized radiation $Q = I_0 \cos 2\theta$ and $U = I_0 \sin 2\theta$, measured with the narrow-beam equipment, using the antenna pattern of the wider-beam equipment as a weighting function. Expressed in brightness temperatures, the Stokes parameters for the wide-beam equipment are:

$$Q' = \overline{T}_b^p \cos 2\theta' = \frac{1}{\Omega'} \int_{\Omega'} f(\theta, \varphi)\, T_b^p \cos 2\theta \, d\Omega ,$$

$$U' = \overline{T}_b^p \sin 2\theta' = \frac{1}{\Omega'} \int_{\Omega'} f(\theta, \varphi)\, T_b^p \sin 2\theta \, d\Omega .$$

The resultant polarization temperature is then $\sqrt{(Q')^2 + (U')^2}$ and the polarization angle is $\theta' = \frac{1}{2} \arctan \frac{Q'}{U'}$.

To compare measurements at different frequencies, we must allow for the frequency-dependence both of the emitted intensity and of the polarization angle, the latter due to the change in Faraday rotation with frequency. We shall assume a spectral index of 2.7, while assumptions about the Faraday rotation will be specified later.

Comparison of our results with those of PAULINY-TOTH *et al.* (1961, methods *i*, *ii*, and *iii*) is impossible due to the fact that their beamwidth in one direction was much smaller than ours, and their frequency well below 200 Mc/s. Comparison with THOMSON (1957) and RAZIN (1958) is impossible due to their very large beamwidths and low frequencies. HARTING (1961, also PAWSEY and HARTING 1960) used a 7° beam at 215 Mc/s and observed at declination −34°, which we cannot reach. We may calculate what polarization temperature he would have found at our two brightest regions (Table 7), for which calculation we shall use the following two models:

a) The Faraday rotation is zero everywhere.

b) In all directions within the 7° beam the polarization angles at emission were equal, and the differences we observe at 408 Mc/s are due entirely to Faraday rotation between the source and us.

TABLE 7

Polarization temperatures predicted for a 7° beam at 215 Mc/s for our two brightest regions, using two different models for the interstellar Faraday rotation.

Region	Position	*a*	*b*
I	$l^{II} = 8°$, $b^{II} = +64°$	16.4 °K	3.8 °K
II	$l^{II} = 140°$, $b^{II} = +7°$	23.2 °K	1.9 °K

The calculations based on model a) give the maximum polarization temperature which could possibly be observed with HARTING's equipment, while model b) is probably more realistic. In practice the region producing the Faraday rotation will not be entirely between the source and us, but the two regions will be partly coincident. In this case, the resultant polarization temperature will be lower still (a reduction of the values of model b) by a factor 5 seems quite possible), but strongly dependent on the exact assumptions made, so that a calculation is of little value.

HARTING's upper limit of 1.5 °K is thus quite compatible with our observations, even in our two brightest regions. We found two such regions in belts along the sky whose total length is some 500°. HARTING's observations extend along about 130°, so that the probability of his finding a similar bright region seems fairly small.

PAULINY-TOTH *et al.* (1961, methods *iv* and *v*) used a beamwidth of 8° at 408 Mc/s. They obtain an upper limit of 2 °K at $\delta = +17°$, $\alpha = 195°$ to 255°. Our results suggest that at $\delta = +14°$, $\alpha = 217°$ ($l^{II} = 8°$, $b^{II} = +64°$, region I above), they would have measured a polarization temperature of 2.7 °K and a polarization angle $\theta = 123°$. At $\delta = +17°$, $\alpha = 217°$ ($l^{II} = 14°$, $b^{II} = +65°$), where we have not enough observations to give a more definite value, and anywhere else where our results overlap theirs, they should probably measure considerably less than their upper limit of 2 °K. We further calculate that they should measure 4.1 °K, with $\theta = 37°$, at region II.

Recent measurements by SHAKESHAFT (*private communication*), using a beamwidth of 8° at 408 Mc/s and a power difference receiver, yield an upper limit of the polarization temperature of 2 °K at $\delta = +14°$, $\alpha = 217°$. At present this seems to be in direct conflict with our results. One possible cause of this is that we did not have enough measurements to fill the 8° beam completely uniformly, but we do not think this will affect our estimate much.

REFERENCES

H. Alfvén and N. Herlofson 1950, *Phys. Rev.* **78**, 616.
H. Bremmer 1949, "Terrestrial Radio Waves", Elsevier, Amsterdam.
I. C. Browne, J. V. Evans, J. K. Hargreaves and W. A. S. Murray 1956, *Proc. Phys. Soc. B* **69**, 901.
M. M. Davis, Louise Volders and Gart Westerhout 1962, *B.A.N.*, in preparation.
J. V. Evans 1956, *Proc. Phys. Soc. B* **69**, 953.
J. V. Evans and G. N. Taylor 1961, *Proc. Roy. Soc. A* **263**, 189.
V. L. Ginsburg 1951, *Dokl. Akad. Nauk. S.S.S.R.* **76**, 377.
V. L. Ginsburg 1953, *Uspekhi Fiz. Nauk.* **51**, 343.
J. S. Hall 1958, *Publ. U.S. Naval Obs.* 2nd series, **17**, 275.
E. Harting 1961, *C.S.I.R.O. Report R.P.R.* 140.
H. C. van de Hulst 1961, *Versl. Afd. Natuurk. Kon. Ned. Ak. Wet., Amsterdam*, **70**, 23.
K.O. Kiepenheuer 1950, *Phys. Rev.* **79**, 738.
E. Le Roux 1961, *Ann. d'Ap.* **24**, 71.
C. H. Mayer, T. P. McCullough and R. M. Sloanaker 1957, *Ap. J.* **126**, 468.
C. H. Mayer, T. P. McCullough and R. M. Sloanaker 1960, U.R.S.I., 13th Assembly, London.
S. K. Mitra 1948, "The Upper Atmosphere", Roy. As. Soc. Bengal, Calcutta.
I. I. K. Pauliny-Toth, J. E. Baldwin and J. R. Shakeshaft 1961, *Monthly Notices R.A.S.* **122**, 279.
J. L. Pawsey and E. Harting 1960, *Austr. J. Phys.* **13**, 740.
V. A. Razin 1958, *Astr. Zhurnal* **35**, 241 (translation: *Soviet Astronomy*: *A. J.* **2**, 216, 1959).
Ch. L. Seeger 1956, *B.A.N.* **13**, 100 (No. 472).
Ch. L. Seeger, G. Westerhout, T. Hoekema and R. G. Conway 1962, *B.A.N., in preparation.*
Ch. L. Seeger, G. Westerhout and H. C. van de Hulst 1959, *B.A.N.* **13**, 89 (No. 472).
I. S. Shklovski 1960, "Cosmic Radio Waves", Harvard Univ. Press, Cambridge, Mass.
C. P. Sonett, D. L. Judge, A. R. Sims and J. M. Kelso 1960, *J. Geoph. Res.* **65**, 55.
J. M. Thomson 1957, *Nature* **180**, 495.
J. A. Van Allen, C. E. McIlwain and G. H. Ludwig 1959, *J. Geoph. Res.* **64**, 271.
J. A. Van Allen 1959, *Nature* **184**, 219.
J. Veldkamp 1951, *Dutch Meteorological Institute, K.N.M.I., De Bilt, Report* No. 134.
S. N. Vernov, A. Ye. Chudakov, P. V. Vakulov and Ye. I. Logachev 1959, *Dokl. Akad. Nauk. S.S.S.R.* **125**, 304.
G. Westerhout 1958, *B.A.N.* **14**, 215 (No. 488).
K. C. Westfold 1959, *Ap. J.* **130**, 241.